Searches for New Physics in Events with a Photon and b–quark Jet at CDF

(September 29, 2001)

T. Affolder,[23] H. Akimoto,[45] A. Akopian,[37] M. G. Albrow,[11] P. Amaral,[8] D. Amidei,[25] K. Anikeev,[24] J. Antos,[1] G. Apollinari,[11] T. Arisawa,[45] A. Artikov,[9] T. Asakawa,[43] W. Ashmanskas,[8] F. Azfar,[30] P. Azzi-Bacchetta,[31] N. Bacchetta,[31] H. Bachacou,[23] S. Bailey,[16] P. de Barbaro,[36] A. Barbaro-Galtieri,[23] V. E. Barnes,[35] B. A. Barnett,[19] S. Baroiant,[5] M. Barone,[13] G. Bauer,[24] F. Bedeschi,[33] S. Belforte,[42] W. H. Bell,[15] G. Bellettini,[33] J. Bellinger,[46] D. Benjamin,[10] J. Bensinger,[4] A. Beretvas,[11] J. P. Berge,[11] J. Berryhill,[8] A. Bhatti,[37] M. Binkley,[11] D. Bisello,[31] M. Bishai,[11] R. E. Blair,[2] C. Blocker,[4] K. Bloom,[25] B. Blumenfeld,[19] S. R. Blusk,[36] A. Bocci,[37] A. Bodek,[36] W. Bokhari,[32] G. Bolla,[35] Y. Bonushkin,[6] D. Bortoletto,[35] J. Boudreau,[34] A. Brandl,[27] S. van den Brink,[19] C. Bromberg,[26] M. Brozovic,[10] E. Brubaker,[23] N. Bruner,[27] E. Buckley-Geer,[11] J. Budagov,[9] H. S. Budd,[36] K. Burkett,[16] G. Busetto,[31] A. Byon-Wagner,[11] K. L. Byrum,[2] S. Cabrera,[10] P. Calafiura,[23] M. Campbell,[25] W. Carithers,[23] J. Carlson,[25] D. Carlsmith,[46] W. Caskey,[5] A. Castro,[3] D. Cauz,[42] A. Cerri,[33] A. W. Chan,[1] P. S. Chang,[1] P. T. Chang,[1] J. Chapman,[25] C. Chen,[32] Y. C. Chen,[1] M. -T. Cheng,[1] M. Chertok,[5] G. Chiarelli,[33] I. Chirikov-Zorin,[9] G. Chlachidze,[9] F. Chlebana,[11] L. Christofek,[18] M. L. Chu,[1] Y. S. Chung,[36] C. I. Ciobanu,[28] A. G. Clark,[14] A. Connolly,[23] J. Conway,[38] M. Cordelli,[13] J. Cranshaw,[40] R. Cropp,[41] R. Culbertson,[11] D. Dagenhart,[44] S. D'Auria,[15] F. DeJongh,[11] S. Dell'Agnello,[13] M. Dell'Orso,[33] L. Demortier,[37] M. Deninno,[3] P. F. Derwent,[11] T. Devlin,[38] J. R. Dittmann,[11] A. Dominguez,[23] S. Donati,[33] J. Done,[39] M. D'Onofrio,[33] T. Dorigo,[16] N. Eddy,[18] K. Einsweiler,[23] J. E. Elias,[11] E. Engels, Jr.,[34] R. Erbacher,[11] D. Errede,[18] S. Errede,[18] Q. Fan,[36] R. G. Feild,[47] J. P. Fernandez,[11] C. Ferretti,[33] R. D. Field,[12] I. Fiori,[3] B. Flaugher,[11] G. W. Foster,[11] M. Franklin,[16] J. Freeman,[11] J. Friedman,[24] H. J. Frisch,[8] Y. Fukui,[22] I. Furic,[24] S. Galeotti,[33] A. Gallas,[(**) 16] M. Gallinaro,[37] T. Gao,[32] M. Garcia-Sciveres,[23] A. F. Garfinkel,[35] P. Gatti,[31] C. Gay,[47] D. W. Gerdes,[25] P. Giannetti,[33] V. Glagolev,[9] D. Glenzinski,[11] M. Gold,[27] J. Goldstein,[11] I. Gorelov,[27] A. T. Goshaw,[10] Y. Gotra,[34] K. Goulianos,[37] C. Green,[35] G. Grim,[5] P. Gris,[11] L. Groer,[38] C. Grosso-Pilcher,[8] M. Guenther,[35] G. Guillian,[25] J. Guimaraes da Costa,[16] R. M. Haas,[12] C. Haber,[23] S. R. Hahn,[11] C. Hall,[16] T. Handa,[17] R. Handler,[46] W. Hao,[40] F. Happacher,[13] K. Hara,[43] A. D. Hardman,[35] R. M. Harris,[11] F. Hartmann,[20] K. Hatakeyama,[37] J. Hauser,[6] J. Heinrich,[32] A. Heiss,[20] M. Herndon,[19] C. Hill,[5] K. D. Hoffman,[35] C. Holck,[32] R. Hollebeek,[32] L. Holloway,[18] R. Hughes,[28] J. Huston,[26] J. Huth,[16] H. Ikeda,[43] J. Incandela,[11] G. Introzzi,[33] J. Iwai,[45] Y. Iwata,[17] E. James,[25] M. Jones,[32] U. Joshi,[11] H. Kambara,[14] T. Kamon,[39] T. Kaneko,[43] K. Karr,[44] H. Kasha,[47] Y. Kato,[29] T. A. Keaffaber,[35] K. Kelley,[24] M. Kelly,[25] R. D. Kennedy,[11] R. Kephart,[11] D. Khazins,[10] T. Kikuchi,[43] B. Kilminster,[36] B. J. Kim,[21] D. H. Kim,[21] H. S. Kim,[18] M. J. Kim,[21] S. B. Kim,[21] S. H. Kim,[43] Y. K. Kim,[23] M. Kirby,[10] M. Kirk,[4] L. Kirsch,[4] S. Klimenko,[12] P. Koehn,[28] K. Kondo,[45] J. Konigsberg,[12] A. Korn,[24] A. Korytov,[12] E. Kovacs,[2] J. Kroll,[32] M. Kruse,[10] S. E. Kuhlmann,[2] K. Kurino,[17] T. Kuwabara,[43] A. T. Laasanen,[35] N. Lai,[8] S. Lami,[37] S. Lammel,[11] J. Lancaster,[10] M. Lancaster,[23] R. Lander,[5] A. Lath,[38] G. Latino,[33] T. LeCompte,[2] A. M. Lee IV,[10] K. Lee,[40] S. Leone,[33] J. D. Lewis,[11] M. Lindgren,[6] T. M. Liss,[18] J. B. Liu,[36] Y. C. Liu,[1] D. O. Litvintsev,[11] O. Lobban,[40] N. Lockyer,[32] J. Loken,[30] M. Loreti,[31] D. Lucchesi,[31] P. Lukens,[11] S. Lusin,[46] L. Lyons,[30] J. Lys,[23] R. Madrak,[16] K. Maeshima,[11] P. Maksimovic,[16] L. Malferrari,[3] M. Mangano,[33] M. Mariotti,[31] G. Martignon,[31] A. Martin,[47] J. A. J. Matthews,[27] J. Mayer,[41] P. Mazzanti,[3] K. S. McFarland,[36] P. McIntyre,[39] E. McKigney,[32] M. Menguzzato,[31] A. Menzione,[33] C. Mesropian,[37] A. Meyer,[11] T. Miao,[11] R. Miller,[26] J. S. Miller,[25] H. Minato,[43] S. Miscetti,[13] M. Mishina,[22] G. Mitselmakher,[12] N. Moggi,[3] E. Moore,[27] R. Moore,[25] Y. Morita,[22] T. Moulik,[35] M. Mulhearn,[24] A. Mukherjee,[11] T. Muller,[20] A. Munar,[33] P. Murat,[11] S. Murgia,[26] J. Nachtman,[6] V. Nagaslaev,[40] S. Nahn,[47] H. Nakada,[43] I. Nakano,[17] C. Nelson,[11] T. Nelson,[11] C. Neu,[28] D. Neuberger,[20] C. Newman-Holmes,[11] C.-Y. P. Ngan,[24] H. Niu,[4] L. Nodulman,[2] A. Nomerotski,[12] S. H. Oh,[10] Y. D. Oh,[21] T. Ohmoto,[17] T. Ohsugi,[17] R. Oishi,[43] T. Okusawa,[29] J. Olsen,[46] W. Orejudos,[23] C. Pagliarone,[33] F. Palmonari,[33] R. Paoletti,[33] V. Papadimitriou,[40] D. Partos,[4] J. Patrick,[11] G. Pauletta,[42] M. Paulini,[(*) 23] C. Paus,[24] L. Pescara,[31] T. J. Phillips,[10] G. Piacentino,[33] K. T. Pitts,[18] A. Pompos,[35] L. Pondrom,[46] G. Pope,[34] M. Popovic,[41] F. Prokoshin,[9] J. Proudfoot,[2] F. Ptohos,[13] O. Pukhov,[9] G. Punzi,[33] A. Rakitine,[24] F. Ratnikov,[38] D. Reher,[23] A. Reichold,[30] A. Ribon,[31] W. Riegler,[16] F. Rimondi,[3] L. Ristori,[33] M. Riveline,[41] W. J. Robertson,[10] A. Robinson,[41] T. Rodrigo,[7] S. Rolli,[44] L. Rosenson,[24] R. Roser,[11] R. Rossin,[31] A. Roy,[35] A. Ruiz,[7] A. Safonov,[12] R. St. Denis,[15] W. K. Sakumoto,[36] D. Saltzberg,[6] C. Sanchez,[28] A. Sansoni,[13] L. Santi,[42] H. Sato,[43] P. Savard,[41] P. Schlabach,[11] E. E. Schmidt,[11] M. P. Schmidt,[47] M. Schmitt,[(**) 16] L. Scodellaro,[31] A. Scott,[6] A. Scribano,[33] S. Segler,[11] S. Seidel,[27] Y. Seiya,[43] A. Semenov,[9] F. Semeria,[3] T. Shah,[24] M. D. Shapiro,[23] P. F. Shepard,[34] T. Shibayama,[43] M. Shimojima,[43] M. Shochet,[8] A. Sidoti,[31] J. Siegrist,[23] A. Sill,[40] P. Sinervo,[41] P. Singh,[18] A. J. Slaughter,[47] K. Sliwa,[44] C. Smith,[19] F. D. Snider,[11] A. Solodsky,[37] J. Spalding,[11] T. Speer,[14] P. Sphicas,[24] F. Spinella,[33] M. Spiropulu,[16] L. Spiegel,[11] J. Steele,[46] A. Stefanini,[33] J. Strologas,[18] F. Strumia,[14] D. Stuart,[11] K. Sumorok,[24] T. Suzuki,[43] T. Takano,[29] R. Takashima,[17] K. Takikawa,[43] P. Tamburello,[10] M. Tanaka,[43] B. Tannenbaum,[6] M. Tecchio,[25] R. Tesarek,[11] P. K. Teng,[1] K. Terashi,[37] S. Tether,[24] A. S. Thompson,[15] R. Thurman-Keup,[2] P. Tipton,[36] S. Tkaczyk,[11] D. Toback,[39] K. Tollefson,[36] A. Tollestrup,[11]

D. Tonelli,[33] H. Toyoda,[29] W. Trischuk,[41] J. F. de Troconiz,[16] J. Tseng,[24] N. Turini,[33] F. Ukegawa,[43] T. Vaiciulis,[36] J. Valls,[38] S. Vejcik III,[11] G. Velev,[11] G. Veramendi,[23] R. Vidal,[11] I. Vila,[7] R. Vilar,[7] I. Volobouev,[23] M. von der Mey,[6] D. Vucinic,[24] R. G. Wagner,[2] R. L. Wagner,[11] N. B. Wallace,[38] Z. Wan,[38] C. Wang,[10] M. J. Wang,[1] B. Ward,[15] S. Waschke,[15] T. Watanabe,[43] D. Waters,[30] T. Watts,[38] R. Webb,[39] H. Wenzel,[20] W. C. Wester III,[11] A. B. Wicklund,[2] E. Wicklund,[11] T. Wilkes,[5] H. H. Williams,[32] P. Wilson,[11] B. L. Winer,[28] D. Winn,[25] S. Wolbers,[11] D. Wolinski,[25] J. Wolinski,[26] S. Wolinski,[25] S. Worm,[27] X. Wu,[14] J. Wyss,[33] W. Yao,[23] G. P. Yeh,[11] P. Yeh,[1] J. Yoh,[11] C. Yosef,[26] T. Yoshida,[29] I. Yu,[21] S. Yu,[32] Z. Yu,[47] A. Zanetti,[42] F. Zetti,[23] and S. Zucchelli[3]

(CDF Collaboration)

[1] *Institute of Physics, Academia Sinica, Taipei, Taiwan 11529, Republic of China*
[2] *Argonne National Laboratory, Argonne, Illinois 60439*
[3] *Istituto Nazionale di Fisica Nucleare, University of Bologna, I-40127 Bologna, Italy*
[4] *Brandeis University, Waltham, Massachusetts 02254*
[5] *University of California at Davis, Davis, California 95616*
[6] *University of California at Los Angeles, Los Angeles, California 90024*
[7] *Instituto de Fisica de Cantabria, CSIC-University of Cantabria, 39005 Santander, Spain*
[8] *Enrico Fermi Institute, University of Chicago, Chicago, Illinois 60637*
[9] *Joint Institute for Nuclear Research, RU-141980 Dubna, Russia*
[10] *Duke University, Durham, North Carolina 27708*
[11] *Fermi National Accelerator Laboratory, Batavia, Illinois 60510*
[12] *University of Florida, Gainesville, Florida 32611*
[13] *Laboratori Nazionali di Frascati, Istituto Nazionale di Fisica Nucleare, I-00044 Frascati, Italy*
[14] *University of Geneva, CH-1211 Geneva 4, Switzerland*
[15] *Glasgow University, Glasgow G12 8QQ, United Kingdom*
[16] *Harvard University, Cambridge, Massachusetts 02138*
[17] *Hiroshima University, Higashi-Hiroshima 724, Japan*
[18] *University of Illinois, Urbana, Illinois 61801*
[19] *The Johns Hopkins University, Baltimore, Maryland 21218*
[20] *Institut für Experimentelle Kernphysik, Universität Karlsruhe, 76128 Karlsruhe, Germany*
[21] *Center for High Energy Physics: Kyungpook National University, Taegu 702-701; Seoul National University, Seoul 151-742; and SungKyunKwan University, Suwon 440-746; Korea*
[22] *High Energy Accelerator Research Organization (KEK), Tsukuba, Ibaraki 305, Japan*
[23] *Ernest Orlando Lawrence Berkeley National Laboratory, Berkeley, California 94720*
[24] *Massachusetts Institute of Technology, Cambridge, Massachusetts 02139*
[25] *University of Michigan, Ann Arbor, Michigan 48109*
[26] *Michigan State University, East Lansing, Michigan 48824*
[27] *University of New Mexico, Albuquerque, New Mexico 87131*
[28] *The Ohio State University, Columbus, Ohio 43210*
[29] *Osaka City University, Osaka 588, Japan*
[30] *University of Oxford, Oxford OX1 3RH, United Kingdom*
[31] *Universita di Padova, Istituto Nazionale di Fisica Nucleare, Sezione di Padova, I-35131 Padova, Italy*
[32] *University of Pennsylvania, Philadelphia, Pennsylvania 19104*
[33] *Istituto Nazionale di Fisica Nucleare, University and Scuola Normale Superiore of Pisa, I-56100 Pisa, Italy*
[34] *University of Pittsburgh, Pittsburgh, Pennsylvania 15260*
[35] *Purdue University, West Lafayette, Indiana 47907*
[36] *University of Rochester, Rochester, New York 14627*
[37] *Rockefeller University, New York, New York 10021*
[38] *Rutgers University, Piscataway, New Jersey 08855*
[39] *Texas A&M University, College Station, Texas 77843*
[40] *Texas Tech University, Lubbock, Texas 79409*
[41] *Institute of Particle Physics, University of Toronto, Toronto M5S 1A7, Canada*
[42] *Istituto Nazionale di Fisica Nucleare, University of Trieste/ Udine, Italy*
[43] *University of Tsukuba, Tsukuba, Ibaraki 305, Japan*
[44] *Tufts University, Medford, Massachusetts 02155*
[45] *Waseda University, Tokyo 169, Japan*
[46] *University of Wisconsin, Madison, Wisconsin 53706*

[47] *Yale University, New Haven, Connecticut 06520*
(*) *Now at Carnegie Mellon University, Pittsburgh, Pennsylvania 15213*
(**) *Now at Northwestern University, Evanston, Illinois 60208*

We have searched for evidence of physics beyond the standard model in events that include an energetic photon and an energetic b-quark jet, produced in 85 pb^{-1} of $\bar{p}p$ collisions at 1.8 TeV at the Tevatron Collider at Fermilab. This signature, containing at least one gauge boson and a third-generation quark, could arise in the production and decay of a pair of new particles, such as those predicted by Supersymmetry, leading to a production rate exceeding standard model predictions. We also search these events for anomalous production of missing transverse energy, additional jets and leptons (e, μ and τ), and additional b-quarks. We find no evidence for any anomalous production of γb or $\gamma b+X$ events. We present limits on two supersymmetric models: a model where the photon is produced in the decay $\tilde{\chi}_2^0 \rightarrow \gamma\tilde{\chi}_1^0$, and a model where the photon is produced in the neutralino decay into the Gravitino LSP, $\tilde{\chi}_1^0 \rightarrow \gamma\tilde{G}$. We also present our limits in a model–independent form and test methods of applying model–independent limits.

PACS number(s): 13.85.Rm, 13.85.Qk, 14.80.Ly

I. INTRODUCTION

As the world's highest–energy accelerator, the Tevatron Collider provides a unique opportunity to search for evidence of physics beyond the standard model. There are many possible additions to the standard model, such as extra spatial dimensions, additional quark generations, additional gauge bosons, quark and lepton substructure, weak–scale gravitational effects, new strong forces, and/or supersymmetry, which may be accessible at the TeV mass scale. In addition, the source of electro-weak symmetry breaking, also below this mass scale, could well be more complicated than the standard model Higgs mechanism.

New physics processes are expected to involve the production of heavy particles,which can decay into standard model constituents (quarks, gluons, and electroweak bosons) which in turn decay to hadrons and leptons. Due to the large mass of the new parent particles, the decay products will be observed with large momentum transverse to the beam (p_t), where the rate for standard model particle production is suppressed. In addition, in many models these hypothetical particles have large branching ratios into photons, leptons, heavy quarks or neutral non-interacting particles, which are relatively rare at large values of p_t in ordinary proton-antiproton collisions.

In this paper we present a broad search for phenomena beyond those expected in the standard model by measuring the production rate of events containing at least one gauge boson, in this case the photon, and a third-generation quark, the b-quark, both with and without additional characteristics such as missing transverse energy ($\not\!\!E_t$). Accompanying searches are made within these samples for anomalous production of jets, leptons, and additional b-quarks, which are predicted in models of new physics. In addition, the signature of one gauge-boson plus a third-generation quark is rare in the standard model, and thus provides an excellent channel in which to search for new production mechanisms.

The initial motivation of this analysis was a search for the stop squark ($\tilde{t}$) stemming from the unusual $ee\gamma\gamma\not\!\!E_t$ event observed at the Collider Detector at Fermilab (CDF) [1]. A model was proposed [2] that produces the photon from the radiative decay of the $\tilde{\chi}_2^0$ neutralino, selected to be the photino, into the $\tilde{\chi}_1^0$, selected to be the orthogonal state of purely higgsino, and a photon. The production of a chargino-neutralino pair, $\tilde{\chi}_i^+\tilde{\chi}_2^0$, could produce the $\gamma b\not\!\!E_{\rm t}$ final state via the decay chain

$$\tilde{\chi}_i^+\tilde{\chi}_2^0 \rightarrow (\tilde{t}b)(\gamma\tilde{\chi}_1^0) \rightarrow (bc\tilde{\chi}_1^0)(\gamma\tilde{\chi}_1^0). \tag{1}$$

This model, however, represents only a small part of the available parameter space for models of new physics. Technicolor models, supersymmetric models in which supersymmetry is broken by gauge interactions, models of new heavy quarks, and models of compositness predicting an excited b quark which decays to γb, for example, would also create this signature. We have consequently generalized the search, emphasizing the signature (γb or $\gamma b\not\!\!E_{\rm t}$) rather than this specific model. We present generalized, model–independent limits. Ideally, these generic limits could be applied to actual models of new physics to provide the information on whether models are excluded or allowed by the data. Other procedures for signature–based limits have been presented recently [1,3,4].

In the next section we begin with a description of the data selection followed by a description of the calculation of backgrounds and observations of the data. Next we present rigorously–derived limits on both Minimal Supersymmetric (MSSM) and Gauge-mediated Supersymmetry Breaking (GMSB) Models. The next sections present the model–independent limits. Finally, in the Appendix we present tests of the application of model–independent limits to a variety of models that generate this signature.

A search for the heavy Techniomega, ω_T, in the final state $\gamma + b + jet$, derived from the same data sample, has already been published [5].

II. DATA SELECTION

The data used here correspond to 85 pb^{-1} of $\bar{p}p$ collisions at $\sqrt{s} = 1.8$ TeV. The data sample was collected by triggering on the electromagnetic cluster caused by the photon in the central calorimeter. We use 'standard' photon identification cuts developed for previous photon analyses [1], which are similar to standard electron requirements except that there is a restriction on any tracks near the cluster. The events are required to have at least one jet with a secondary vertex found by the standard silicon detector b–quark identification algorithm. Finally, we apply missing transverse energy requirements and other selections to examine subsamples. We discuss the selection in detail below.

A. The CDF Detector

We briefly describe the relevant aspects of the CDF detector [6]. A superconducting solenoidal magnet provides a 1.4 T magnetic field in a volume 3 m in diameter and 5 m long, containing three tracking devices. Closest to the beamline is a 4-layer silicon microstrip detector (SVX) [7] used to identify the secondary vertices from b–hadron decays. A track reconstructed in the SVX has an impact parameter resolution of 19μm at high momentum to approximately 25μm at 2 GeV/c of track momentum. Outside the SVX, a time projection chamber (VTX) locates the z position of the interaction. In the region with radius from 30 cm to 132 cm, the central tracking chamber (CTC) measures charged–particle momenta. Surrounding the magnet coil is the electromagnetic calorimeter, which is in turn surrounded by the hadronic calorimeter. These calorimeters are constructed of towers, subtending 15° in ϕ and 0.1 in η [8], pointing to the interaction region. The central preradiator wire chamber (CPR) is located on the inner face of the calorimeter in the central region ($|\eta| < 1.1$). This device is used to determine if the origin of an electromagnetic shower from a photon was in the magnet coil. At a depth of six radiation lengths into the electromagnetic calorimeter (and 184 cm from the beamline), wire chambers with additional cathode strip readout (central electromagnetic strip chambers, CES) measure two orthogonal profiles of showers.

For convenience we report all energies in GeV, all momenta as momentum times c in GeV, and all masses as mass times c^2 in GeV. Transverse energy (E_t) is the energy deposited in the calorimeter multiplied by $\sin\theta$.

B. Event Selection

Collisions that produce a photon candidate are selected by at least one of a pair of three-level triggers, each of which requires a central electromagnetic cluster. The dominant high–E_t photon trigger requires a 23 GeV cluster with less than approximately 5 GeV additional energy in the region of the calorimeter surrounding the cluster [9]. A second trigger, designed to have high efficiency at large values of E_t, requires a 50 GeV cluster, but has no requirement on the isolation energy.

These events are required to have no energy deposited in the hadronic calorimeter outside of the time window that corresponds to the beam crossing. This rejects events where the electromagnetic cluster was caused by a cosmic ray muon which scatters and emits bremsstrahlung in the calorimeter.

Primary vertices for the $\bar{p}p$ collisions are reconstructed in the VTX system. A primary vertex is selected as the one with the largest total $|p_t|$ attached to it, followed by adding silicon tracks for greater precision. This vertex is required to be less than 60 cm from the center of the detector along the beamline, so that the jet is well-contained and the projective nature of the calorimeters is preserved.

C. Photon

To purify the photon sample in the offline analysis, we select events with an electromagnetic cluster with E_t >25 GeV and $|\eta| < 1.0$. To provide for a reliable energy measurement we require the cluster to be away from cracks in the calorimeter. To remove backgrounds from jets and electrons, we require the electromagnetic cluster to be isolated. Specifically, we require that the shower shape in the CES chambers at shower maximum be consistent with that of a single photon, that there are no other clusters nearby in the CES, and that there is little energy in the hadronic calorimeter towers associated with (*i.e.* directly behind) the electromagnetic towers of the cluster.

We allow no tracks with $p_t > 1$ GeV to point at the cluster, and at most one track with $p_t < 1$ GeV. We require that the sum of the p_t of all tracks within a cone of $\Delta R = \sqrt{\Delta\eta^2 + \Delta\phi^2} = 0.4$ around the cluster be less than 5 GeV.

If the photon cluster has $E_t < 50$ GeV, we require the energy in a 3×3 array of trigger towers (trigger towers are made of two consecutive physical towers in η) to be less than 4 GeV. This isolation energy sum excludes the energy in the electromagnetic calorimeter trigger tower with the largest energy. This requirement is more restrictive than the hardware trigger isolation requirement, which is approximately 5 GeV on the same quantity. In some cases the photon shower leaks into adjacent towers and the leaked photon shower energy is included in the isolation energy sum. This effect leads to an approximately 20% inefficiency for this trigger. When the cluster E_t is above 50 GeV, a second trigger with no isolation requirement accepts the event. For these events, we require the transverse energy found in the calorimeter in a cone of $R = 0.4$ around the cluster to be less than 10% of the cluster's energy.

These requirements yield a data sample of 511,335 events in an exposure of 85 pb^{-1} of integrated luminosity.

D. B-quark Identification

Jets in the events are clustered with a cone of 0.4 in $\eta - \phi$ space using the standard CDF algorithm [10]. One of the jets with $|\eta| < 2$ is required to be identified as a b–quark jet by the displaced-vertex algorithm used in the top–quark analysis [11]. This algorithm searches for tracks in the SVX that are associated with the jet but not associated with the primary vertex, indicating they come from the decay of a long–lived particle. We require that the track, extrapolated to the interaction vertex, has a distance of closest approach greater than 2.5 times its uncertainty and pass loose requirements on p_t and hit quality. The tracks passing these cuts are used to search for a vertex with three or more tracks. If no vertex is found, additional requirements are placed on the tracks, and this new list is used to search for a two–track vertex. The transverse decay length, L_{xy}, is defined in the transverse plane as the projection of the vector pointing from the primary vertex to the secondary vertex on a unit vector along the jet axis. We require $|L_{xy}|/\sigma > 3$, where σ is the uncertainty on L_{xy}. These requirements constitute a "tag". In the data sample the tag is required to be positive, with $L_{xy} > 0$. The photon cluster can have tracks accidentally associated with it and could possibly be tagged; we remove these events. This selection reduces the dataset to 1487 events.

The jet energies are corrected for calorimeter gaps and non-linear response, energy not contained in the jet cone, and underlying event energy [10]. For each jet the resulting corrected E_t is the best estimate of the underlying true quark or gluon transverse energy, and is used for all jet requirements in this analysis. We require the E_t of the tagged jet in the initial $b\gamma$ event selection to be greater than 30 GeV; this reduces the data set to 1175 events.

E. Other Event Selection

While the photon and b–tagged jet constitute the core of the signature we investigate, supersymmetry and other new physics could be manifested in any number of different signatures. Because of the strong dependence of signature on the many parameters in supersymmetry, one signature is (arguably) not obviously more likely than any other. For these reasons we search for events with unusual properties such as very large missing E_t or additional reconstructed objects. These objects may be jets, leptons, additional photons or b-tags. This method of sifting events was employed in a previous analysis [1]. We restrict ourselves to objects with large E_t since this process is serving as a sieve of the events for obvious anomalies. In addition, in the lower E_t regime the backgrounds are larger and more difficult to calculate. In this section we summarize the requirements that define these objects.

Missing E_t ($\not\!\!E_t$) is the magnitude of negative of the two-dimensional vector sum of the measured E_t in each calorimeter tower with energy above a low threshold in the region $|\eta| < 3.6$. All jets in the event with uncorrected E_t greater than 5 GeV and $|\eta| <2$ are corrected appropriately for known systematic detector mismeasurements; these corrections are propagated into the missing E_t. Missing E_t is also corrected using the measured momentum of muons, which do not deposit much of their energy in the calorimeter.

We apply a requirement of 20 GeV on missing E_t, and observe that a common topology of the events is a photon opposite in azimuth from the missing E_t (see Figure 2). We conclude that a common source of missing E_t occurs when the basic event topology is a photon recoiling against a jet. This topology is likely to be selected by the $\not\!\!E_t$ cut because the fluctuations in the measurement of jet energy favor small jet energy over large. To remove this background, we remove events in the angular bin $\Delta\phi(\gamma - \not\!\!E_t) > 168°$ for the sample, where we have raised the missing E_t requirement to 40 GeV.

We define H_t as the scalar sum of the E_t in the calorimeter added to the missing E_t and the p_t of any muons in the event. This would serve as a measure of the mass scale of new objects that might be produced.

To be recognized as an additional jet in the event, a calorimeter cluster must have corrected E_t >15 GeV and $|\eta| < 2$. To count as an additional b tag, a jet must be identified as a b candidate by the same algorithm as the primary b jet, and have $E_t > 30$ GeV and $|\eta| <2$. To be counted as an additional photon, an electromagnetic cluster is required to have $E_t > 25$ GeV, $|\eta| < 1.0$, and to pass all the same identification requirements as the primary photon.

Object	Selection
Basic Sample Requirements	
Isolated Photon	$E_t > 25$ GeV, $\lvert\eta\rvert < 1.0$
b-quark jet (SVX b-tag)	$E_t > 30$ GeV, $\lvert\eta\rvert < 2.0$
Optional Missing E_t Requirements	
$\not\!\!E_t$	> 40 GeV
$\lvert\Delta\phi(\gamma - \not\!\!E_t)\rvert$	$< 168°$
Optional Other Objects	
Jets	$E_t > 15$ GeV, $\lvert\eta\rvert < 2.0$
Additional Photons	$E_t > 25$ GeV, $\lvert\eta\rvert < 1.0$
Additional b-quark jets	$E_t > 30$ GeV, SVX b-tag
Electrons	$E_t > 25$ GeV, $\lvert\eta\rvert < 1.0$
Muons	$p_t > 25$ GeV, $\lvert\eta\rvert < 1.0$
Tau Leptons	$E_t > 25$ GeV, $\lvert\eta\rvert < 1.2$

TABLE I. Summary of the kinematic selection criteria for the $b\gamma + X$ sample that contains 1175 events. Also shown are the kinematic criteria for the identification of other objects, such as missing E_t, jets, additional b-jets and leptons. The lepton identification criteria are the same as used in the top discovery.

For lepton identification, we use the cuts defined for the primary leptons in the top quark searches [11,12]. We search for electrons in the central calorimeter and for muons in the central muon detectors. Candidates for τ leptons are identified only by their hadronic decays – as a jet with one or three high–p_t charged tracks, isolated from other tracks and with calorimeter energy cluster shapes consistent with the τ hypothesis [12]. Electrons and τ's must have $E_t > 25$ GeV as measured in the calorimeter; muons must have $p_t > 25$ GeV. Electrons and muons must have $|\eta| < 1.0$ while τ's must have $|\eta| < 1.2$. We summarize the kinematic selections in Table I.

III. BACKGROUND ESTIMATES

The backgrounds to the $b\gamma$ sample are combinations of standard model production of photons and b quarks and also jets misidentified as a photon ("fake" photons) or as a b–quark jet ("fake" tags or mistags). A jet may be misidentified as a photon by fragmenting to a hard leading π^0. Other jets may fake a b–quark jet through simple mismeasurement of the tracks leading to a false secondary vertex.

We list these backgrounds and a few other smaller backgrounds in Table II. The methods referred to in this table are explained in the following sections.

Source	Method of Calculation
$\gamma b\bar{b}$ and $\gamma c\bar{c}$	Monte Carlo
$\gamma+$ mistag	CES–CPR and tagging prediction
fake γ and bb or $c\bar{c}$	CES–CPR
fake γ and a mistag	CES–CPR
$W\gamma$, $Z\gamma$	Monte Carlo, normalized to data
electrons faking γ's	measured fake rate
cosmic rays	cosmic characteristics

TABLE II. The summary of the backgrounds to the photon and tag sample and the methods used to calculate them.

The following sections begin with a discussion of the tools used to calculate backgrounds. Section III C explains why the method presented is necessary. The subsequent sections provide details of the calculation of each background in turn.

A. Photon Background Tools

There are two methods we use to calculate photon backgrounds, each used in a different energy region. The first employs the CES detector embedded at shower maximum in the central electromagnetic calorimeter [13]. This method is based on the fact that the two adjacent photons from a high–p_t π^0 will tend to create a wide CES cluster, with a larger CES χ^2, when compared to the single photon expectation. The method produces an event-by-event weight based on the χ^2 of the cluster and the respective probabilities to find this χ^2 for a π^0 versus for a photon. In the decay of very high–energy π^0's the two photons will overlap, and the π^0 will become indistinguishable from a single photon in the CES by the shape of the cluster. From studies of π^0's from ρ decay we have found that for $E_t > 35$ GeV the two photons coalesce and we must use a second method of discrimination that relies on the central preradiator system (CPR) [13]. This background estimator is based on the fact that the two photons from a π^0 have two chances to convert to an electron-positron pair at a radius before the CPR system, versus only one chance for a single photon. The charged particles from the conversion leave energy in the CPR, while an unconverted photon does not. The implementation of the CPR method of discriminating photons from π^0's on a statistical basis is similar to the CES method, an event-by-event weight. When the two methods are used together to cover the entire photon E_t range for a sample, we refer to it as the CES–CPR method.

Both these photon background methods have low discrimination power at high photon E_t. This occurs because the weights for a single photon and a (background) π^0 are not very different. For example, in the CES method, at an E_t of 25 GeV, the probability for a photon to have a large χ^2 is on the order of 20% while the background has a probability of approximately 45%. For the CPR method, typical values for a 25 GeV photon are 83% conversion probability for background and 60% for a single photon.

B. b-quark Tagging Background Tools

A control sample of QCD multi-jet events is used to study the backgrounds to the identification of b–quark jets [14]. For each jet in this sample, the E_t of the jet, the number of SVX tracks associated with the jet, and the scalar sum of the E_t in the event are recorded. The probability of tagging the jet is determined as a function of these variables for both positive ($L_{xy} > 0$) and negative tags ($L_{xy} < 0$).

Negative tags occur due to measurement resolution and errors in reconstruction. Since these effects produce negative and positive tags with equal probability, the negative tagging probability can be used as the probability of finding a positive tag due to mismeasurement (mistags).

C. Background Method

We construct a total background estimate from summing the individual sources of backgrounds, each found by different methods. In the CDF top analysis [11] one of the tagging background procedures was to apply the positive tagging probability to the jets in the untagged sample to arrive at a total tagging background estimate. A similar procedure could be considered for our sample.

However, in this analysis, a more complex background calculation is necessary for two reasons. First, the parameterized tagging background described above is derived from a sample of jets from QCD events [11] which have a different fraction of b–quark jets than do jets in a photon-plus-jets sample. This effect is caused by the coupling of the photon to the quark charge. Secondly, b quarks produce B mesons which have a large branching ratio to semileptonic states that include neutrinos, producing real missing E_t more often than generic jets. When a $\not\!\!E_t$ cut is applied, the b fraction tends to increase. This effect is averaged over in the positive background parameterization so the background prediction will tend to be high at small $\not\!\!E_t$ and low at large $\not\!\!E_t$.

For these reasons, the positive tagging rate is correlated to the existence of a photon and also the missing E_t, when that is required. In contrast, the negative tagging rate is found not to be significantly correlated with the presence of real b quarks. This is because the negative tagging rate is due only to mismeasurement of charged tracks which should not be sensitive to the flavor of the quarks.

The next sections list the details of the calculations of the individual sources of the backgrounds. Both photons and b–tagged jets have significant backgrounds so we consider sources with real photons and b–tags or jets misidentified as photons or b–jets ("fakes").

D. Heavy Flavor Monte Carlo

The background consisting of correctly–identified photons and b–quark jets is computed with an absolutely normalized Monte Carlo [15]. The calculation is leading order, based on $q\bar{q}$ and gg initial states and a finite b–quark mass. The Q^2 scale is taken to be the square of the photon E_t plus the square of the $b\bar{b}$ or $c\bar{c}$ pair mass, $Q^2 = E_t^2 + M^2$. A systematic uncertainty of 30% is found by scaling Q by a factor of two and the quark masses by 10%. An additional 20% uncertainty allows for additional effects which cannot be determined by simply changing the scale dependence [15].

In addition, we rely on the detector simulation of the Monte Carlo to predict the tail of the rapidly falling $\not\!\!E_t$ spectrum. The Monte Carlo does not always predict this tail well. For example, a Monte Carlo of $Z \to e^+e^-$ production predicts only half the observed rate for events passing the missing E_t cut used in this analysis. We thus include an uncertainty of 100% on the rate that events in the $b\gamma$ sample pass the $\not\!\!E_t$ cut. We combine the Monte Carlo production and $\not\!\!E_t$ sources of uncertainty in quadrature. However when the $\gamma b\bar{b}$ and $\gamma c\bar{c}$ backgrounds are totaled, these common uncertainties are treated as completely correlated.

E. Fake photons

The total of all backgrounds with fake photons can be measured using the CES and CPR detectors. These backgrounds, dominated by jets that fragment to an energetic $\pi^0 \to \gamma\gamma$ and consequently are misidentified as a single photon, are measured using the shower shape in the CES system for photon $E_t < 35$ GeV and the probability of a conversion before the CPR for $E_t > 35$ GeV [16]. We find $55 \pm 1 \pm 15\%$ [17] of these photon candidates are actually jets misidentified as photons.

For many of our subsamples we find this method is not useful due to the large statistical dilution as explained in Section III. This occurs because, for example, the probabilities for background (π^0's) and for signal (γ's) to convert before the CPR are not too different. This results in a weak separation and a poor statistical uncertainty. We find the method returns 100% statistical uncertainties for samples of less than approximately 25 photon candidates.

F. Real photon, Fake tags

To estimate this background we start with the untagged sample, and weight it with both the CES-CPR real photon weight and the negative tagging (background) weight. This results in the number of true photons with mistags in the final sample. As discussed above, the negative tagging prediction does not have the correlation to quark flavor and missing E_t as does the positive tagging prediction.

As a check, we can look at the sample before the tagging and $\not\!\!E_t$ requirements. In this sample we find 197 negative tags while the estimate from the negative tagging prediction is 312. This discrepancy could be due to the topology of the events – unlike generic jets, the photon provides no tracks to help define the primary vertex. The primary vertex could be systematically mismeasured leading to mismeasurement of the transverse decay length L_{xy} for some events. We include a 50% uncertainty on this background due to this effect.

G. Estimate of Remaining Backgrounds

There are several additional backgrounds which we have calculated and found to very small. The production of $W\gamma$ and $Z\gamma$ events may provide background events since they produce real photons and b or c quarks from the boson decay ($W^\pm \to c\bar{s}$, $Z \to b\bar{b}$). The $\not\!\!E_t$ would have to be fake, due to mismeasurement in the calorimeter. We find $W/Z\gamma$ events in the CDF data using the same photon requirements as the search. The W/Z is required to decay leptonically for good identification. We then use a Monte Carlo to measure the ratio of the number of these events to the number of events passing the full $\gamma b\not\!\!E_t$ search cuts. The product of these two numbers predicts this background to be less than 0.1 events.

The next small background is $W \to e\nu$ plus jets where the electron track is not reconstructed, due either to bremsstrahlung or to pattern-recognition failure. Using $Z \to e^+e^-$ events, we find this probability is small, about 0.5%. Applying this rate to the number of observed events with an electron, b-tag and missing E_t we find the number of events expected in our sample to be negligible.

The last small background calculation is the rate for cosmic ray events. In this case there would have to be a QCD b–quark event with a cosmic ray bremsstrahlung in time with the event. The missing E_t comes with the unbalanced energy deposited by the cosmic ray. We use the probability that a cosmic ray leaves an unattached stub in the muon chambers to estimate that the number of events in this category is also negligible.

The total of all background sources is summarized in Table III. The number of observed events is consistent with the calculation of the background for both the γb sample and the subsamples with $\not\!\!E_t$.

IV. DATA OBSERVATIONS

In this section we report the results of applying the final event selection to the data. First we compare the total background estimate with the observed number of events in the $b\gamma$ sample, which requires only a photon with $E_t > 25$ GeV and a b–tagged jet with $E_t > 30$ GeV. Since most models of supersymmetry predict missing E_t, we also tabulate the backgrounds for that subsample.

Table III summarizes the data samples and the predicted backgrounds. We find 98 events have missing $E_t > 20$ GeV. Six events have missing $E_t > 40$ GeV, and only two of those events pass the $\Delta\phi(\gamma - \not\!\!E_t) < 168^\circ$ cut.

Figures 1 and 2 display the kinematics of the data with a background prediction overlayed. Because of the large statistical uncertainty in the fake photon background, the prediction for bins with small statistics have such large uncertainties that they are not useful. In this case we approximate the fake photon background by applying the fake photon measurement and the positive tagging prediction to the large-statistics untagged sample. This approximation only assumes that real b quarks do not produce substantial missing E_t. Each component of the background is normalized to the number expected as shown in Table III; the total is then normalized to the data in order to compare distributions. We observe no significant deviations from the expected background.

Source	Events	Events $\not\!\!E_t > 20$	Events $\not\!\!E_t > 40$, $\Delta\phi$
γbb	$99 \pm 5 \pm 50$	$9 \pm 1 \pm 10$	$0.4 \pm 0.3 \pm 0.4$
$\gamma c\bar{c}$	$161 \pm 9 \pm 81$	$7 \pm 2 \pm 8$	$0.0 \pm 0.5 \pm 0.5$
γ+mistag	$124 \pm 1 \pm 62$	$10 \pm 0.3 \pm 5.2$	$0.7 \pm 0.05 \pm 0.5$
fake γ	$648 \pm 69 \pm 94$	$49 \pm 22 \pm 7$	$1.0 \pm 1.0 \pm 0.2$
$W\gamma$	2 ± 1	$0.4 \pm 0.2 \pm 0.4$	$0.0 \pm 0.1 \pm 0.1$
$Z\gamma$	6 ± 4	$0.8 \pm 0.6 \pm 0.8$	$0.08 \pm 0.06 \pm 0.08$
$e \to \gamma$	0.4 ± 0.1	0.4 ± 0.1	$0.1 \pm .03$
cosmics	0 ± 16	0 ± 5	0
total background	$1040 \pm 72 \pm 172$	$77 \pm 23 \pm 20$	$2.3 \pm 1.2 \pm 1.1$
data	1175	98	2

TABLE III. Summary of the primary background calculation. The $\gamma b\bar{b}$ and $\gamma c\bar{c}$ systematic uncertainties are considered 100% correlated. The column labeled $\not\!\!E_t > 40$ GeV also includes the requirement that $\Delta\phi(\gamma - \not\!\!E_t) < 168^\circ$. The entry for fake photons in the column labeled $\not\!\!E_t > 40$ GeV is not measured but is estimated using the assumption that 50% of photons are fakes. This number is assigned a 100% uncertainty.

Several events appear on the tails of some of the distributions. Since new physics, when it first appears, will likely be at the limit of our kinematic sensitivity, the tail of any kinematic distribution is a reasonable place to look for anomalous events. However, a few events at the kinematic limit do not warrant much interest unless they have many characteristics in common or they have additional unusual properties. We find two events pass the largest missing E_t cut of 40 GeV; we examine those events more closely below. We also observe there are five events with large dijet mass combinations and we also look at those more closely below. In Section IV C, we search for other anomalies in our sample.

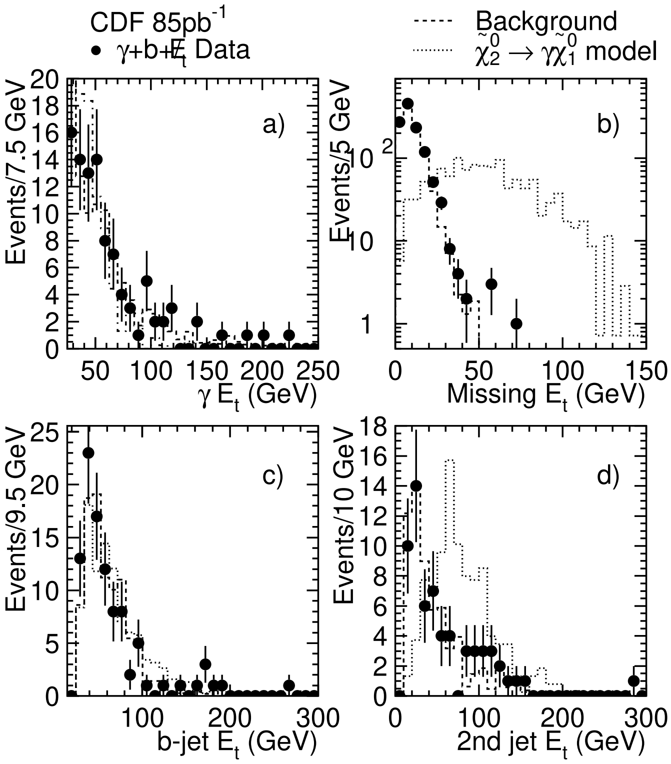

FIG. 1. Comparison of the data to the background prediction (dashed line), and the baseline SUSY model of Section V A 2 (dotted line). The data consist of the 98 events of the γb data with $\not\!\!E_t > 20$ GeV, except in b) which contains no $\not\!\!E_t$ requirement. In each case the predictions have been normalized to the data. The distributions are: a) the photon E_t, b) the missing E_t, c) the b–tagged jet E_t and d) the E_t of the second jet with E_t >15 GeV, if there is one. For display, the SUSY model event yield is scaled up by a factor of 4 for a), c) and d) and a factor of 40 for b).

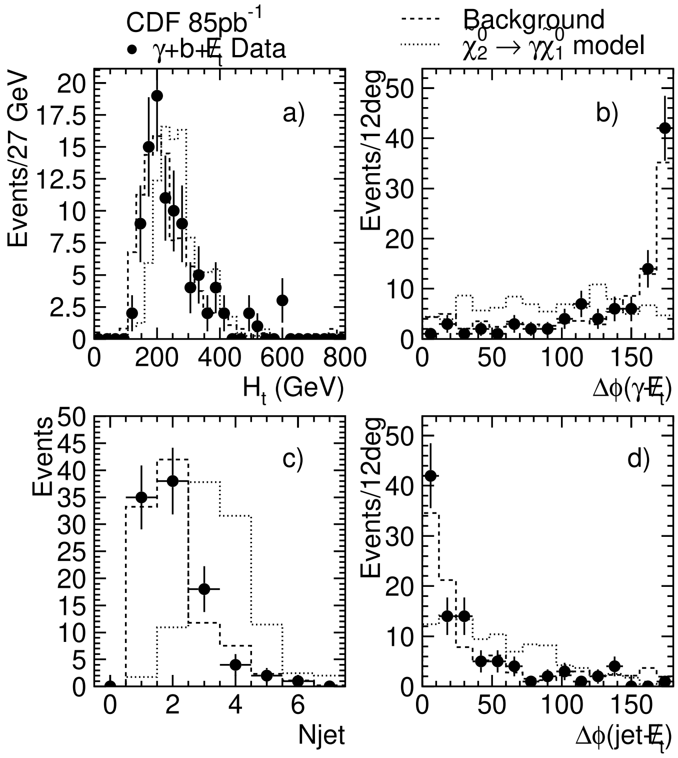

FIG. 2. Comparison of the data to the background prediction (dashed line), and the the baseline SUSY model of Section V A 2 (dotted line), each normalized to the 98 events of the γb data with $\not\!\!E_t > 20$ GeV. The distributions are: a) H_t (total energy), b) $\Delta\phi$ between the photon and the $\not\!\!E_t$, c) number of jets with $E_t > 15$ GeV, and d) $\Delta\phi$ between the missing E_t and the nearest jet. For display, the SUSY model event yield is scaled up by a factor of 4.

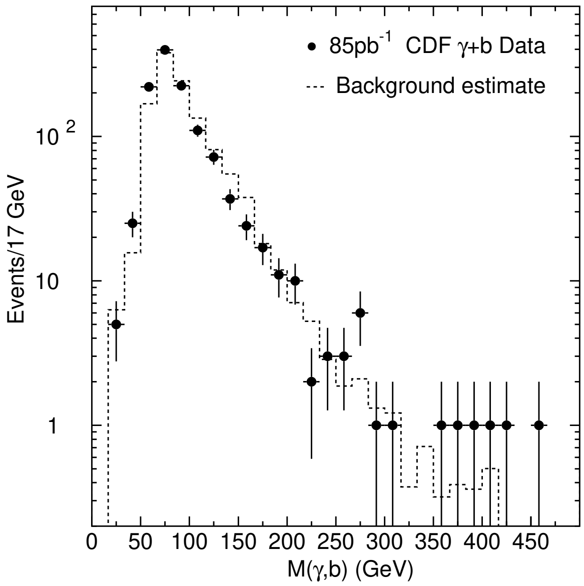

FIG. 3. Comparison of the γb mass in the data to the background prediction (dashed line), normalized to the 1175 events of the γb data.

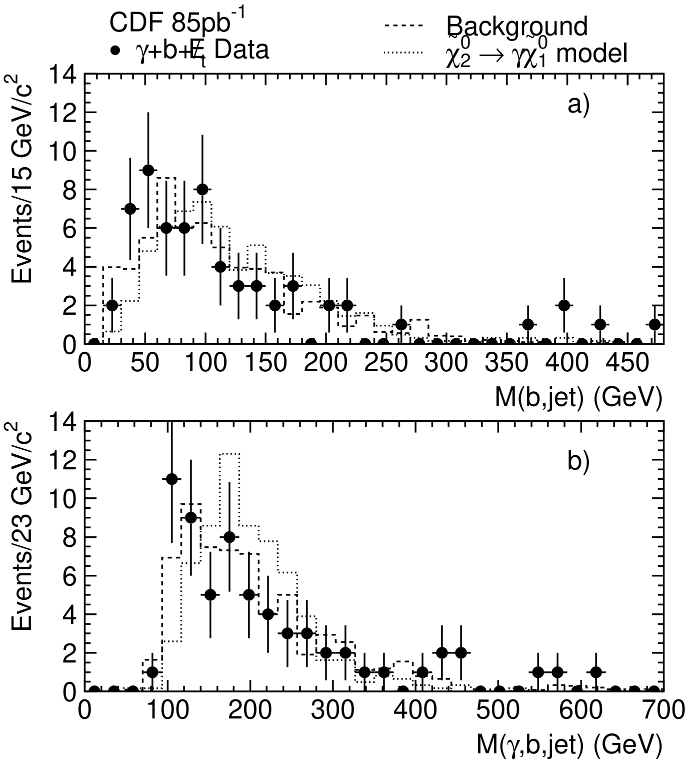

FIG. 4. The distributions for: a) $M(b,j)$ and b) $M(\gamma,b,j)$ for the $\not\!\!E_t > 20$ GeV events as shown in Figure 5. Only 63 of the 98 events have a second jet and make it into this plot. The data are compared to a background prediction (dashed line), and the baseline SUSY model of Section V A 2 (dotted line), each normalized to the data. The Monte Carlo prediction is scaled up by a factor of 3.

A. Analysis of Events with Large Missing E_t

Six events pass the *a priori* selection criteria requiring a photon, b–tag, and $\not\!\!E_t$ >40 GeV. Two of these events also pass the $\Delta\phi(\gamma - \not\!\!E_t) < 168°$ requirement. We have examined these two events to see if there indications of anything else unusual about them (for example, a high–p_t lepton, or a second jet which forms a large invariant mass with the first b-jet, to take signals of GMSB and Higgsino models respectively).

The first event (67537/59517) does not have the characteristics of a typical b-tag. It is a two-track tag (which has a worse signal–to–noise) with the secondary vertex consistent with the beam pipe radius (typical of an interaction in the beam pipe). The two tracks have a p_t of 2 and 60 GeV, respectively; this highly asymmetric configuration is unlikely if the source is a b–jet. There are several other tracks at the same ϕ as the jet that are inconsistent with either the primary or secondary vertex. We conclude the b-tag jet in this event is most likely to be a fake, coming from an interaction in the beam pipe.

The second event has a typical b–tag but there are three jets, and all three straddle cracks in the calorimeter ($\eta = 0.97, -1.19, -0.09$), implying the $\not\!\!E_t$ is very likely to be mismeasured.

In both events we judge by scanning that the primary vertex is the correct choice so that a mismeasurement of the $\not\!\!E_t$ due to selecting the wrong vertex is unlikely.

While we have scanned these two events and find they are most likely not true $\gamma b \not\!\!E_t$ events, we do not exclude them from the event sample as the background calculations include these sources of mismeasured events.

Run/Event	γ E_t	$\not\!\!E_t$	$M(b, jet)$	b E_t	jets E_t	$\Delta\phi(\gamma - \not\!\!E_t)$	$\Delta\phi(j_{near} - \not\!\!E_t)$	H_t
60951/189718	121	42	57	61	67,26,15	177	11	342
64997/119085	222	44	97	173	47	170	1	495
63684/15166	140	57	63	35	25,20,15	175	6	388
67537/59517*	36	73	399	195	141,113,46,17	124	20	595
69426/104696	33	58	266	143	119	180	3	344
68464/291827*	93	57	467	128	155,69	139	16	405

TABLE IV. Characteristics of the six events with $\not\!\!E_t$ > 40 GeV; the two marked with an asterisk also pass the $\Delta\phi(\gamma - \not\!\!E_t) < 168°$ requirement. All units are GeV except for $\Delta\phi$ which is in degrees. The columns are the E_t of the photon in the event, the missing E_t, the mass of the b-jet and the second highest E_t jet in the event, the E_t of the b jet, the E_t of the jets other than the b jet, the $\Delta\phi$ between the photon and the missing E_t, the $\Delta\phi$ between the the missing E_t and the nearest jet, and the H_t of the event (scalar sum of the E_t, the missing E_t and the p_t of any muons in the event).

B. Analysis of Five High–mass Events

If the events include production of new, heavy particles, we might observe peaks, or more likely, distortions in the distributions of the masses formed from combinations of objects. To investigate this, we create a scatter plot of the mass of the b-quark jet and the second highest-E_t jet versus the mass of the photon, b-quark jet and second highest jet in Figure 5 and 4.

As seen in the figures, the five events at highest $M(b, j)$ seem to form a cluster on the tail of the distribution. There are 63 events in the scatter plot which are the subset of the 98 events with $\not\!\!E_t > 20$ GeV which contain a second jet. The five events include the two (probable background) events with $\not\!\!E_t > 40$ GeV and $\Delta\phi(\gamma - \not\!\!E_t) < 168°$ and three events with large H_t (> 400 GeV). Since these events were selected for their high mass, we expect they would appear in the tails of several of the distributions such as H_t. Table V shows the characteristics of these five events.

Run/Event	γ E_t	$\not\!\!E_t$	$M(b, jet)$	b E_t	jet E_t's	$\Delta\phi(\gamma - \not\!\!E_t)$	$\Delta\phi(j_{near} - \not\!\!E_t)$	H_t
66103/52684	106	24	433	170	135,57	152	29	517
66347/373704	122	32	369	268	125,42	101	14	605
67537/59517	36	73	399	195	141,113,46,17	124	20	595
68333/233128	38	39	395	99	282,212	121	3	600
68464/291827	93	57	467	128	155,69	139	16	405

TABLE V. Characteristics of events with $M(b, jet) > 300$ GeV. For a complete description of the quantities, see Table IV.

In order to see if these events are significant, we need to make an estimate of the expected background. We define the two regions indicated in Figure 5. The small box is placed so that it is close to the five events.[1] This is intended to maximize the significance of the excess. The large box is placed so that it is as far from the five events as possible without including any more data events. This will minimize the significance. The two boxes can serve as informal upper and lower bounds on the significance. Since these regions were chosen based on the data, the excess over background cannot be used to prove the significance of these events. These estimates are intended only to give a guideline for the significance.

We cannot estimate the background to these five events using the CES and CPR methods described in Section III A due to the large inherent statistical uncertainties in these techniques. We instead use the following procedure. The list of backgrounds in Section III defines the number of events from each source with no restriction on $M(b,j)$. We normalize these numbers to the 63 events in the scatter plot. We next derive the fraction of each of these sources we expect at high $M(b,j)$. We multiply the background estimates by the fractions. The result is a background estimate for the high–mass regions.

To derive the fractions of background sources expected at high $M(b,j)$ we look at each background in turn. The fake photons are QCD events where a jet has fluctuated into mostly electromagnetic energy. For this source we use the positive L_{xy} background prediction [11] to provide the fraction. This prediction is derived from a QCD jet sample by parameterizing the positive tagging probability as a function of several jet variables. The probability for each jet is summed over all jets for the untagged sample to arrive at a tagging prediction. Since the prediction is derived from QCD jets we expect it to be reliable for these QCD jets also. Running this algorithm (called "Method 1" [11]) on the untagged photon and $\not\!\!E_t$ sample yields the fraction of expected events in each of the two boxes. The fractions are summarized in Table VI.

Source	Big box	Small box
fake γ	0.080 ± 0.007	0.017 ± 0.003
γ, fake tag	0.112 ± 0.009	0.032 ± 0.005
γbb	0.10 ± 0.03	0.022 ± 0.007
$\gamma c\bar{c}$	0.08 ± 0.04	0.018 ± 0.008

TABLE VI. The fraction of the 63 $\gamma bj\not\!\!E_t$ events for each background expected to fall into the high–$M(b,j)$ boxes defined in Figure 5.

[1]Note that events cannot be above the diagonal in the $M(\gamma,b,j) - M(b,j)$ plane, so the true physical area is triangular.

The second background source considered consists of real photons with fake tags. We calculate this contribution using the measured negative tagging rate applied to all jets (i.e. before b-tagging) in the sample. Finally, the real photon and heavy flavor backgrounds are calculated based on the Monte Carlo. The results from estimating the fractions are shown in Table VI.

The estimates of the sources of background for the 63 events at all $M(b,j)$ have statistical uncertainties, as do the fractions in Table VI; we include both in the uncertainty in the number of events in the high–mass boxes. We propagate the systematic uncertainties on the backgrounds to the 63 events at all $M(b,j)$ and include the following systematics due to the fractions:

1. 50% of the real photon and mistag background calculation for the possibility that the quark and gluon content, as well as the heavy flavor fraction, in photon events may differ from the content in QCD jets.

2. 50% of the real photon and mistag background calculation for the possibility that using the positive tagging prediction to correct the Monte Carlo for the $\not\!\!E_t$ cut may have a bias.

3. 100% of the real photon and real heavy flavor background calculation for the possibility that the tails in the Monte Carlo $M(b,j)$ distribution may not be reliable.

The results of multiplying the backgrounds at all $M(b,j)$ with the fractions expected at high $M(b,j)$ are shown in Table VII.

Source	Big box	Small box
fake γ	$3.3 \pm 1.5 \pm 0.5$	$0.70 \pm 0.33 \pm 0.10$
γ, fake tag	$0.97 \pm 0.09 \pm 0.69$	$0.28 \pm 0.05 \pm 0.20$
γbb	$0.75 \pm 0.26 \pm 1.18$	$0.16 \pm 0.06 \pm 0.26$
$\gamma c\bar{c}$	$0.44 \pm 0.26 \pm 0.79$	$0.11 \pm 0.06 \pm 0.17$
total	$5.5 \pm 1.5 \pm 1.6$	$1.24 \pm 0.35 \pm 0.38$

TABLE VII. Summary of the estimates of the background at high $M(b,j)$ in the boxes in the $M(\gamma,b,j) - M(b,j)$ plane defined in Figure 5.

The result is that we expect $5.5 \pm 1.5 \pm 1.6$ events in the big box, completely consistent with five observed. We expect $1.2 \pm 0.35 \pm 0.38$ events in the small box. The probability of observing five in the small box is 1.6%, a 2.7σ effect, *a posteriori*.

We next address a method for avoiding the bias in deciding where to place a cut when estimating backgrounds to events on the tail of a distribution. This method was developed by the Zeus collaboration for the analysis of the significance of the tail of the Q^2 distribution [18]. Figure 6 summarizes this method. The Poisson probability that the background fluctuated to the observed number of events (including uncertainties on the background estimate) is plotted for different cut values. We use the projection of the scatter plot onto the $M(b,j)$ axis and make the cut on this variable since this is where the effect is largest. We find the minimum probability is 1.4×10^{-3}, which occurs for a cut of $M(b,j)$ >400 GeV. We then perform 10,000 "pseudo-experiments" where we draw the data according to the background distribution derived above and find the minimum probability each time. We find 1.2% of these experiments have a minimum probability lower than the data, corresponding to a 2.7σ fluctuation. Including the effect of the uncertainties in the the background estimate does not significantly change the answer.

We note that this method is one way of avoiding the bias from deciding in what region to compare data and backgrounds after seeing the data distributions. It does not, however, remove the bias from the fact that we are investigating this plot, over all others, because it looks potentially inconsistent with the background. If we make enough plots one of them will have a noticeable fluctuation. We conclude that the five events on the tail represent something less than a 2.7σ effect.

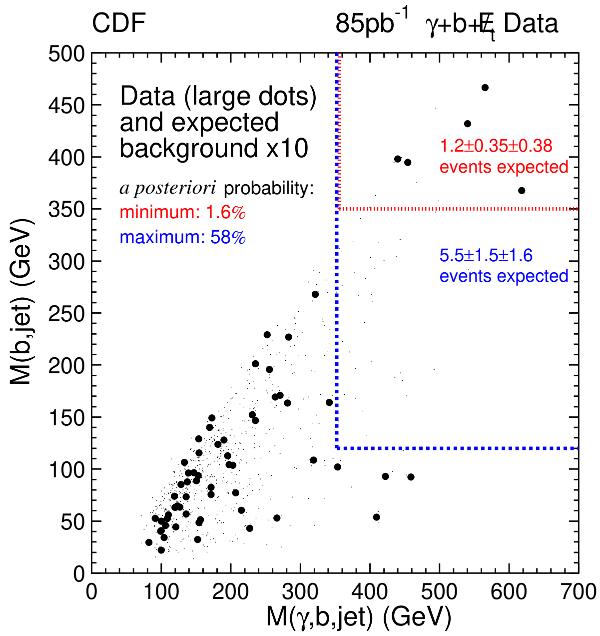

FIG. 5. $M(b,j)$ versus $M(\gamma,b,j)$ for the events with $\not{E}_t > 20$ GeV as shown in Figure 5. Only 63 of the 98 events have a second jet and make it into this plot. The small dots are the result of making the scatter plot for the untagged data (passing all other cuts) and weighting it with the positive tagging prediction. The estimates of background expected in the boxes are found by the method described in the text.

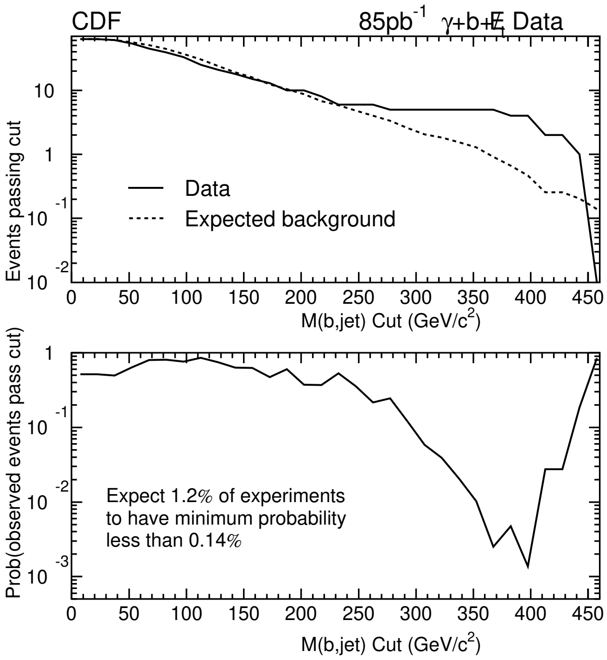

FIG. 6. The upper plot is the number of events passing a cut on $M(b, j)$ for the data and the positive tagging prediction. The lower plot is the probability that the number of events passing a cut on $M(b, j)$ is consistent with the positive tagging prediction. The expected number of experiments with such a low minimum probability is derived from 10,000 simulated experiments drawn from the distribution of the expected background.

C. Additional Objects in the Data Sample

We have searched the γb data sample for other unusual characteristics. The creation and decay of heavy squarks, for example, could produce an excess of events with multiple jets. In Figure 7 we histogram the number of events with N or more jets. Table VIII presents the numbers of events observed and expected. Some backgrounds are negative due to the large statistical fluctuations of the fake photon background. When all backgrounds are included the distribution in the number of jets in the data is consistent with that from background.

Min N_{jet}	Observed, $\not{E}_t > 0$ GeV	Expected, $\not{E}_t > 0$ GeV	Observed, $\not{E}_t > 20$ GeV	Expected, $\not{E}_t > 20$ GeV
1	1175	$1040 \pm 72 \pm 172$	98	$77 \pm 23 \pm 20$
2	464	$394 \pm 44 \pm 63$	63	$39 \pm 18 \pm 12$
3	144	$82 \pm 24 \pm 14$	25	$-8 \pm 12 \pm 3$
4	36	$17 \pm 11 \pm 3$	7	–
5	10	–	3	–
6	5	–	1	–
7	2	–	0	–
8	1	–	0	–

TABLE VIII. Numbers of events with N or more jets and the expected Standard Model background. Some background predictions are negative due to the large statistical fluctuations on the fake photon background method.

We have searched in the sample of events with a photon and b–tagged jet for additional high–E_t objects using the requirements defined in Section II E. We find no events containing a second photon. We find no events containing a hadronic τ decay or a muon. We find one event with an electron; its characteristics are listed in Table IX. In scanning this event, we note nothing else unusual about it.

We find 8 events of the 1175 which have a photon and b–tagged jet contain a second b–tagged jet with E_t >30 GeV. (Out of the 1175, only 200 events have a second jet with E_t >30 GeV.) Unfortunately, this is such a small sample that we cannot use the background calculation to find the expected number of these events (the photon background CES–CPR method returns 100% statistical uncertainties). One of the events with two tags has 30 GeV of missing E_t so is in the 98–event $\not{E}_t > 20$ GeV sample.

Run/Event	γ E_t	$\not{E}_t$	$M(\gamma, e)$	b E_t	electron E_t	$\Delta\phi(\gamma - \not{E}_t)$	H_t
63149/4148	42	17	21	106	33	43	212

TABLE IX. Characteristics of the one event with a photon, tagged jet, and an electron.

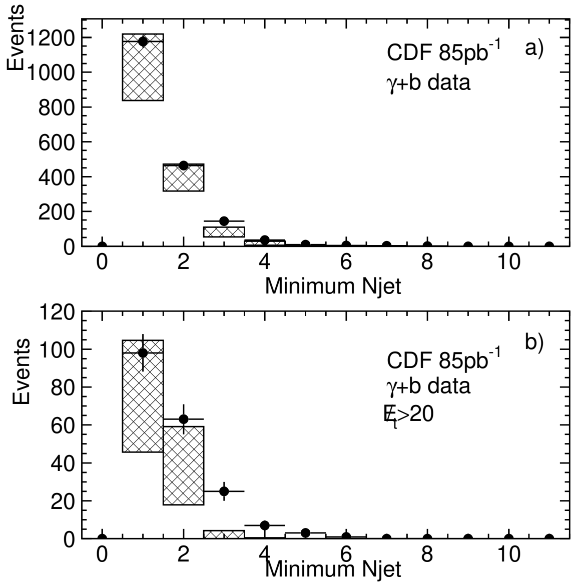

FIG. 7. The distribution of the number of events with N or more jets, represented by the solid points. The boxes are centered on the background prediction and their size reflects plus and minus one-σ of combined statistical and systematic uncertainty on the background prediction. The distributions are: a) all events with a photon and b-tagged jet, b) all events with a photon, b-tagged jet and $\not\!\!E_t > 20$ GeV. Some background predictions are negative due to the large statistical fluctuations on the fake photon background method. The results are also tabulated in Table VIII.

V. LIMITS ON MODELS OF SUPERSYMMETRY

In the following sections we present limits on three specific models of supersymmetry [19]. Each of these models predicts significant numbers of events with a photon, a b–quark jet and missing transverse energy ($i.e\ \gamma b\not\!\!E_t$).

As is typical for supersymmetry models, each of these shows the problems in the process of choosing a model and presenting limits on it. Each of these models is very specific and thus represents a very small area in a very large parameter space. Consequently the odds that any of these is the correct picture of nature is small. They are current theories devised to address current concerns and may appear dated in the future. (This aspect is particularly relevant to the experimentalists, who often publish their data simultaneously with an analysis depending on a current model.) In addition these models can show sensistivity to small changes in the parameters.

The first model is based on a particular location in MSSM parameter space which produces the signature of $\gamma b\not\!\!E_t+X$. We consider both direct production of charginos and neutralinos and, as a second model, indirect production of charginos and neutralinos through squarks and gluinos. The third model is based on the gauge–mediated concept, discussed further below.

A. $\tilde{\chi}_2^0 \to \gamma\tilde{\chi}_1^0$ Model

This theoretical model was originally proposed in the context of the anomalous CDF $ee\gamma\gamma\not\!\!E_t$ event [1,2]. Here, however, we go beyond the constraints of this single event and only retain the essential elements of the model, optimized for CDF detector acceptence and efficiency. This is an MSSM model without any specific relation to a high–energy theory. It does not assume high–energy constraints such as the unification of the sfermion or scalar masses as is assumed in the models inspired by Supergravity (SUGRA) [19]. In this section and the following section we develop a baseline model point in parameter space. The final limits on this model will be found for this point and for some variations around this point.

1. Direct Gaugino Production in $\tilde{\chi}_2^0 \to \gamma\tilde{\chi}_1^0$ Model

The first part of the model [2] is a light stop squark ($\tilde{t}$), the superpartner to the top quark. In this model the $\tilde{\chi}_i^\pm$ then decays to $\tilde{t}b$ and the $\tilde{t}$ decays to $\tilde{\chi}_1^0 c$. The second important feature of the model is the decay $\tilde{\chi}_2^0 \to \gamma\tilde{\chi}_1^0$ which dominates in a particular region of MSSM parameter space. With these decays dominating, any event where a $\tilde{\chi}_i^\pm$ and a $\tilde{\chi}_2^0$ is produced, either directly or indirectly through the strong production and decays of squarks and gluinos, will contain a photon, a b–quark jet and missing E_t.

The heart of the model [2] is the decay $\tilde{\chi}_2^0 \to \gamma\tilde{\chi}_1^0$ so we examine in detail the parameter space where this decay dominates. The branching ratio of this decay is large when one of the neutralinos is a pure photino and one is pure Higgsino. To make a pure photino, we set $M_1 = M_2$. The photino mass is then equal to M_2. To make a pure Higgsino we set $\tan\beta \approx 1$. To avoid the theoretical bias against a very small $\tan\beta$ (which makes the top Yukawa coupling go to infinity before the GUT scale) we will use $\tan\beta = 1.2$. In this case, the Higgsino mass is approximately equal to $|\mu|$. The above is purely a result of the form of the neutralino mass matrix. For definitions of these model parameters and discussions of their roles in SUSY models please see [19].

This leaves two free parameters to define the charginos and neutralinos, M_2 and μ. Figure 8 shows five regions in the $\mu - M_2$ plane; Table X summarizes the regions. First we note that in region 5 ($\mu > 0$) we do not observe the decay $\tilde{\chi}_2^0 \to \gamma\tilde{\chi}_1^0$ because typically $\tilde{\chi}_1^\pm < \tilde{\chi}_2^0$ and $\tilde{\chi}_2^0 \to W^*\tilde{\chi}_1^\pm$.

For $\mu < 0$, there are four regions. In region 2, which is the region suggested in [2], the $\tilde{\chi}_2^0$ is the photino, $\tilde{\chi}_1^0$ is the Higgsino, and the decay $\tilde{\chi}_2^0 \to \gamma\tilde{\chi}_1^0$ dominates. In region 3, $\tilde{\chi}_2^0$ is the Higgsino and $\tilde{\chi}_1^0$ is the photino and the photon decay still dominates. In region 1 the photino has become so heavy it is now the $\tilde{\chi}_3^0$. In region 4, the Higgsino has become the $\tilde{\chi}_3^0$. In regions 3 and 4 it is still possible to get photon decays, sometimes even $\tilde{\chi}_3^0 \to \gamma\tilde{\chi}_2^0$.

Region	$\tilde{\chi}_1^0$	$\tilde{\chi}_2^0$	$\tilde{\chi}_3^0$	$\tilde{\chi}_4^0$
1	$\tilde{h}_b$	$\tilde{Z}$	$\tilde{\gamma}$	$\tilde{h}_a$
2	$\tilde{h}_b$	$\tilde{\gamma}$	$\tilde{Z}$	$\tilde{h}_a$
3	$\tilde{\gamma}$	$\tilde{h}_b$	$\tilde{Z}$	$\tilde{h}_a$
4	$\tilde{\gamma}$	$\tilde{Z}$	$\tilde{h}_b$	$\tilde{h}_a$

TABLE X. The approximate content of the neutralinos in the four regions of the $\mu - M_2$ plane with $\mu < 0$ shown in Figure 8. The symbols $\tilde{h}_a$ and $\tilde{h}_b$ are simply the antisymmetric and symmetric combinations of $\tilde{H}_1^0$ and $\tilde{H}_2^0$ [19].

We choose to concentrate on region 2 where the photon plus b decay signature can be reliably estimated by the Monte Carlo event generator `PYTHIA` [20]. The $\tilde{\chi}_2^0 \to \gamma\tilde{\chi}_1^0$ decay dominates here. We also note that in this region the cross section for $\tilde{\chi}_2^{\pm}\tilde{\chi}_2^0$ is 3–10 times larger than the cross section for $\tilde{\chi}_1^{\pm}\tilde{\chi}_2^0$ even though the $\tilde{\chi}_2^{\pm}$ is significantly heavier than the $\tilde{\chi}_1^{\pm}$. This is due to the large $\tilde{W}$ component of the $\tilde{\chi}_2^{\pm}$.

Since region 2 is approximately one-dimensional, we scan in only one dimension, along the diagonal, when setting limits on $\tilde{\chi}_2^{\pm}\tilde{\chi}_2^0$ production. To decide where in the region to place the model, we note that the mass of $\tilde{\chi}_2^0$ equals M_2 and the mass of $\tilde{\chi}_1^0 = |\mu|$ in this region. To give the photon added boost for a greater sensitivity, we will set M_2 significantly larger than $|\mu|$. This restricts us to the upper part of region 2. The dotted line in Figure 8 is the set of points defined by all these criteria and is given by $M_2 = 0.89 * |\mu| + 39$ GeV.

The next step is to choose a $\tilde{t}$ mass. It is necessary that $\tilde{\chi}_1^0 < \tilde{t} < \tilde{\chi}_1^{\pm}$ for the decay $\tilde{\chi}_1^{\pm}, \tilde{\chi}_2^{\pm} \to b\tilde{t}$ to dominate. We find that in Region 2, $\tilde{\chi}_1^{\pm} \approx M_2$. If the $\tilde{t}$ mass is near the $\tilde{\chi}_1^{\pm}$, the b will only have a small boost, but the $\tilde{\chi}_1^0$ in the decay $\tilde{t} \to c\tilde{\chi}_1^0$ will have a greater boost, giving greater $\not{E}_t$. If the $\tilde{t}$ mass is near the $\tilde{\chi}_1^0$, the opposite occurs. In Monte Carlo studies, we find considerably more sensitivity if the $\tilde{t}$ mass is near the $\tilde{\chi}_1^0$. We set the $\tilde{t}$ mass to be $M_{\tilde{\chi}_1^0} + 5$ GeV. Since the $\tilde{\chi}_2^{\pm}\tilde{\chi}_2^0$ production cross section is larger than $\tilde{\chi}_1^{\pm}\tilde{\chi}_2^0$ and will be detected with better efficiency, when we simulate direct production we set the Monte Carlo program to produce only $\tilde{\chi}_2^{\pm}\tilde{\chi}_2^0$ pairs. The final limit is expressed as a cross section limit plotted versus the $\tilde{\chi}_2^{\pm}$ mass (which is very similar to the $\tilde{\chi}_2^0$ mass). This model is designed to provide a simple, intuitive signature that is not complicated by branching ratios and many modes of production.

For the baseline model, we chose a value of μ near the exclusion boundary of current limits [21] on a $\tilde{t}$ which decays to $c\chi_1^0$. The point we chose is $M_{\tilde{\chi}_1^0} = 80$ GeV. From the above prescription, this corresponds to $M_{\tilde{\chi}_1^0} = -\mu = 80$ GeV, $M_{\tilde{\chi}_2^0} = M_{\tilde{\chi}_1^{\pm}} = M_2 = 110$ GeV, and $M_{\tilde{t}} = 85$ GeV. This point, indicated by the dot in Figure 8, gives the lightest mass spectrum with good mass splittings that is also near the exclusion boundary from LEP and DO Collaborations.

2. Squarks and Gluinos

Now we address the squarks and gluinos, which can produce $\tilde{\chi}_i^{\pm}\tilde{\chi}_2^0$ in their decays, and sleptons, which can appear in the decays of charginos and neutralinos.

We will set the squarks (the lighter $\tilde{b}$ and both left and right $\tilde{u}$, $\tilde{d}$, $\tilde{s}$ and $\tilde{c}$) to 200 GeV and the gluino to 210 GeV. The heavier $\tilde{t}$ and $\tilde{b}$ are above 1 TeV. The gluino will decay to the squarks and their respective quarks. The squarks will decay to charginos or neutralinos and jets. This will maximize the production of $\tilde{\chi}_i^{\pm}\tilde{\chi}_2^0$ and therefore the sensitivity.

This brings us to the limit on indirect production in the $\tilde{\chi}_2^0 \to \gamma\tilde{\chi}_1^0$ model. The chargino and neutralino parameters are fixed at the baseline model parameters. We then vary the gluino mass and set the squark mass according to $M_{\tilde{g}} = M_{\tilde{Q}} + 10$ GeV. The limit is presented as a limit on cross section plotted versus the gluino mass. When the gluino mass crosses the $\tilde{t}\bar{t}$ threshold at 260 GeV, the gluino can decay to $\tilde{t}\bar{t}$ and production of $\tilde{\chi}_i^{\pm}\tilde{\chi}_2^0$ decreases. However, since all squarks are lighter than the gluino, the branching ratio to the $\tilde{t}$ is limited and production will not fall dramatically.

Some remaining parameters of the model are now addressed. Sleptons could play a role in this model. They have small cross sections so they are not often directly produced, but if the sleptons are lighter than the charginos, the charginos can decay into the sleptons. In particular, the chargino decay $\tilde{t}b$ may be strongly suppressed if it competes with a slepton decay. We therefore set the sleptons to be very heavy so they do not compete for branching ratios. We set M_A large. The lightest Higgs turns out to be only 87 GeV due to the corrections from the light third–generation squarks. This is below current limits so we attempted to tune the mass to be heavier and found it was difficult to achieve, given the light $\tilde{t}$ and low $\tan\beta$.

Using the `PYTHIA` Monte Carlo program, we find that 69% of all events generated with squarks and gluinos have the decay $\tilde{\chi}_2^0 \to \gamma\tilde{\chi}_1^0$, 58% have the decay $\tilde{\chi}_i^{\pm} \to \tilde{t}b$, and 30% have both. (To be precise, the light stop squark was excluded from this exercise, as it decays only to $c\chi_1^0$. A light stop pair thus gives the signature $c\bar{c} + \not{E}_t$, one of the signatures used to search for it, [21,22] but not of interest here.)

3. Acceptances and Efficiencies

This section describes the evaluation of the acceptance and efficiency for the indirect production of $\tilde{\chi}_i^{\pm}\tilde{\chi}_i^0$ through squarks and gluinos and the direct production of $\tilde{\chi}_2^{\pm}\tilde{\chi}_2^0$ in the MSSM model of $\tilde{\chi}_2^0 \to \gamma\tilde{\chi}_1^0$. We use the `PYTHIA` Monte Carlo with the CTEQ4L parton distribution functions (PDFs) [23]. The efficiencies for squark and gluino production at the baseline point are listed in Table XI.

Cuts		Cumulative Efficiency (%)
Photon	$E_t > 25$ GeV,$\lvert\eta\rvert < 1.0$, ID cuts	50
One jet	$E_{t,corr} > 30$ GeV, $\lvert\eta\rvert < 2.0$	47
One SVX tag	$E_{t,corr} > 30$ GeV, $\lvert\eta\rvert < 2.0$	4.3
$\not{E}_t$	> 40 GeV	2.9

TABLE XI. Efficiencies for the baseline point with squark and gluino production. The efficiencies do not include branching ratios.

The total efficiencies, which will be used to set production limits below, are listed in Table XII for the production of $\tilde{\chi}_i^{\pm}\tilde{\chi}_i^0$ through squarks and gluinos, and in Table XIII for direction production. Typical efficiencies are 2-3% in the former case, and 1% in the latter.

4. Systematic Uncertainty

Some systematics are common to the indirect production and the direct production. The efficiencies of the isolation requirement in the Monte Carlo and $Z \to e^+e^-$ control sample cannot be compared directly due to differences in the E_t-spectra of the electromagnetic cluster, and the multiplicity and E_t spectra of associated jets. The difference (14%) is taken to be the uncertainty in the efficiency of the photon identification cuts. The systematic uncertainty on the b–tagging efficiency (9%) is the statistical uncertainty in comparisons of the Monte Carlo and data. The systematic uncertainty on the luminosity (4%) reflects the stability of luminosity measurements.

We next evaluate systematics specifically for the indirect production. The baseline parton distribution function is CTEQ4L. Comparing the efficiency with this PDF to the efficiencies obtained with MRSD0$'$ [24] and GRV–94LO [25] for the squark and gluino production, we find a standard deviation of 5%. Turning off initial– and final–state radiation (ISR/FSR) in the Monte Carlo increases the efficiency by 1% and 2% respectively and we take half of these as the respective systematics. Varying the jet energy scale by 10% causes the efficiency to change by 4%. In quadrature, the total systematic for the indirect production is 18%.

Evaluating the same systematics for the direct production, we find the uncertainty from the choice of PDF is 5%, from ISR/FSR is 2%/9%, and from jet energy scale is 4%. In quadrature, the total systematic uncertainty for the direct production is 20%.

5. Limits on the $\tilde{\chi}_2^0 \to \gamma\tilde{\chi}_1^0$ Model, Indirect Production

To calculate an approximate upper limit on the number of $\gamma b \not{E}_t$ events from squark and gluino production, we use the limit implied from the observed 2 events, including the effect of the systematic uncertainties [26,27]. We divide the Poisson probability for observing $\leq$2 events for a given expected signal and background, convoluted with the uncertainties, by the Poisson probability for observing $\leq$2 events for a given background only, also convoluted with the uncertainties. The number of expected signal events is increased until the ratio falls below 5%, leading to an approximate 95% confidence level limit of 6.3 events. Other limits in this paper are computed similarly.

This upper limit, the efficiency described above (also see Table XII), and the luminosity, 85 pb^{-1}, are combined to find the cross section limit for this model. The theoretical cross section is calculated at NLO using the `PROSPINO` program [28]. The effect is to uniformly increase the strong interaction production cross sections by 30% (improving the limit). At the baseline point (including squarks and gluinos) described above, we expect 18.5 events, so this point is excluded. Next we find the limit as a function of the gluino mass. The squark mass is 10 GeV below the gluino mass and the rest of the sparticles are as in the baseline point. We can exclude gluinos out to a mass of 245 GeV in this model. The limits are displayed in Table XII and Figure 9.

$M_{\tilde{g}}(GeV)$	$M_{\tilde{q}}$ (GeV) ,	$\sigma_{th} \times BR$ (pb)	$A\epsilon$ (%)	$\sigma_{95\%\ lim} \times BR$ (pb)
185	175	16.8	1.97	3.76
210	200	7.25	2.98	2.49
235	225	3.49	3.23	2.30
260	250	1.94	2.69	2.76
285	275	1.24	2.16	3.45

TABLE XII. Efficiency times acceptance and limits on indirect production of $\tilde{\chi}_i^{\pm}\tilde{\chi}_2^0$ though squarks and gluinos. Approximately 30% of events contain the decays $\tilde{\chi}_2^0 \to \gamma\tilde{\chi}_1^0$ and $\tilde{\chi}_i^{\pm} \to \tilde{t}b$. The efficiencies in this table are found as the number of events passing all cuts divided by the number of events that contain both of these decays. The product of cross section times branching ratio listed in each case is for all open channels of SUSY production. Masses are given in GeV (following our convention of quoting $M \times c^2$) and cross sections are in pb. The second row is the baseline point.

6. Limits on the $\tilde{\chi}_2^0 \to \gamma\tilde{\chi}_1^0$ Model, Direct Production

In this case the number of observed events (two) is convoluted with the systematic uncertainty to obtain an upper limit of 6.4 events (95% C.L.). To calculate the expected number of events from the direct production of $\tilde{\chi}_2^{\pm}\tilde{\chi}_2^0$, we vary μ, and calculate the $M_{\tilde{t}}$ and M_2 as prescribed above. The results are shown in Table XIII and Figure 10. For these values of the model parameters, the branching ratios $\tilde{\chi}_2^{\pm} \to \tilde{t}b$ and $\tilde{\chi}_2^0 \to \gamma\tilde{\chi}_1^0$ are 100%.

As can be seen from Figure 10, the predicted rates from direct production are smaller than the measured limits by 1-3 orders-of-magnitude, and no mass limit on the $\tilde{\chi}_2^{\pm}$ mass can be set.

$M_{\tilde{\chi}_1^0} = -\mu$	$M_{\tilde{\chi}_2^0} = M_2,$	$M_{\tilde{\chi}_1^{\pm}}$	$M_{\tilde{\chi}_2^{\pm}}$	$M_{\tilde{t}}$	σ_{th}	$A\epsilon$ (%)	$\sigma_{95\%\ lim}$
25	61	71	110	30	0.23	0.93	8.06
62	95	94	130	67	0.034	1.41	5.33
79	110	108	140	85	0.018	1.29	5.85
93	123	118	150	98	0.0075	1.34	5.58
118	146	140	170	123	0.0022	1.27	5.94

TABLE XIII. Efficiencies and limits on direct production of $\tilde{\chi}_2^{\pm}\tilde{\chi}_2^0$. Branching ratios $\tilde{\chi}_2^0 \to \gamma\tilde{\chi}_1^0$ and $\tilde{\chi}_i^{\pm} \to \tilde{t}b \to (\tilde{\chi}_1^0 c)b$ are 100%. Masses are in GeV and the cross sections are in pb. The third row is the baseline point.

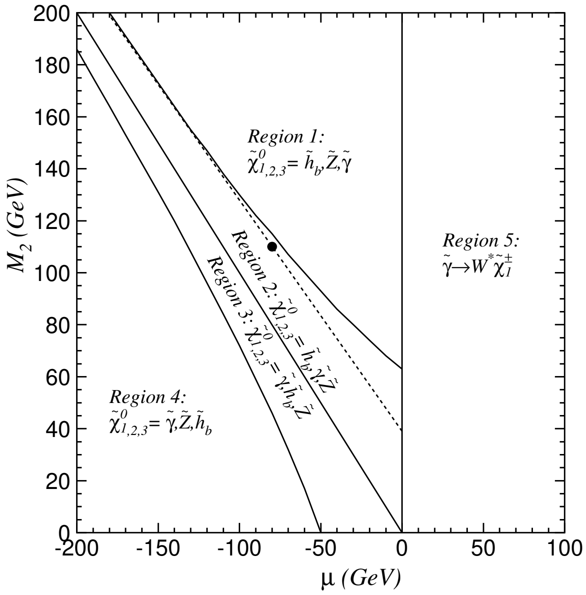

FIG. 8. The five regions in the supersymmetry parameter $M_2 - \mu$ plane where different mass hierarchies occur. The three lightest neutralinos are denoted $\tilde{\chi}^0_{1,2,3}$, respectively. The dashed line is the locus of points scanned for the limits and is given by $M_2 = 0.89|\mu| + 39$ GeV. The dot is the baseline model described in the text.

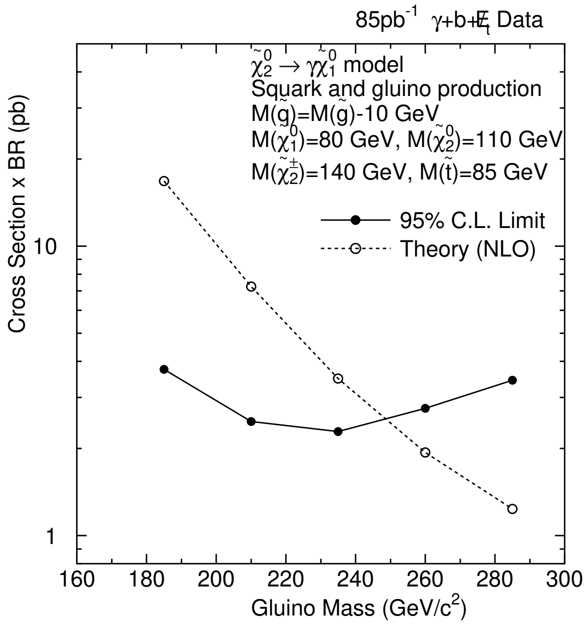

FIG. 9. The limits on the cross section times branching ratio for SUSY production of $\gamma b \not\!\!E_t$ events in the $\tilde{\chi}_2^0 \rightarrow \gamma\tilde{\chi}_1^0$ model. All production processes have been included; the dominant mode is the production of squarks and gluinos which decay to charginos and neutralinos. The overall branching ratio to the $\gamma b \not\!\!E_t$ topology is approximately 30%.

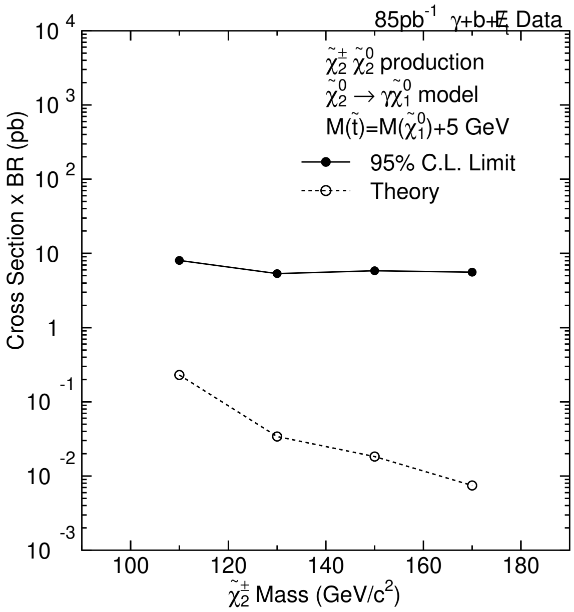

FIG. 10. The limits on the $\tilde{\chi}_2^{\pm}\tilde{\chi}_2^0$ cross section in the $\tilde{\chi}_2^0 \to \gamma\tilde{\chi}_1^0$ SUSY model. The branching ratios $\tilde{\chi}_2^0 \to \gamma\tilde{\chi}_1^0$ and $\tilde{\chi}_i^{\pm} \to \tilde{t}b \to (\tilde{\chi}_1^0 c)b$ are taken to be 100%.

B. Gauge-mediated Model

This is the second SUSY model [19] which can give substantial production of the signature $\gamma b\not\!\!E_t$. In this model the difference between the mass of the standard model particles and their SUSY partners is mediated by gauge (the usual electromagnetic, weak, and strong) interactions [29] instead of gravitational interactions as in SUGRA models. SUSY is assumed broken in a hidden sector. Messenger particles gain mass through renormalization loop diagrams which include the hidden sector. SUSY particles gain their masses through loops which include the messenger particles.

This concept has the consequence that the strongly–interacting squarks and gluinos are heavy and the right-handed sleptons are at the same mass scale as the lighter gauginos. A second major consequence is that the gravitino is very light (eV scale) and becomes the LSP. The source of b quarks is no longer the third generation squarks, but the decays of the lightest Higgs boson. If the lightest neutralino is mostly Higgsino, the decay $\tilde{\chi}_1^0 \rightarrow h\tilde{G}$ can compete with the decays $\tilde{\chi}_1^0 \rightarrow Z\tilde{G}$ and $\tilde{\chi}_1^0 \rightarrow \gamma\tilde{G}$. The Higgs decays to $b\bar{b}$ as usual. Since SUSY particles are produced in pairs, each event will contain two cascades of decays down to two $\tilde{\chi}_1^0$'s, each of which in turn will decay by one of these modes. If one decays to a Higgs and one decays to a photon, the event will have the signature of a photon, at least one b–quark jet, and missing E_t.

We will use a minimal gauge-mediated model with one exception. This MGMSB model has five parameters, with the following values:

- $\Lambda = 61 - 90$ TeV, the effective SUSY-breaking scale;
- $M/\Lambda = 3$, where M is the messenger scale;
- $N = 2$ the number of messenger multiplets;
- $\tan\beta = 3$;
- the sign of $\mu < 0$.

We will compute the MGMSB model using the GMSB option of `ISAJET` [30]. We then re–enter the model using the MSSM options so that we can make one change: we set $\mu = -0.75M_1$. This makes the lightest neutralino a Higgsino so the branching ratio for $\tilde{\chi}_1^0 \rightarrow h\tilde{G}$ will be competitive with $\tilde{\chi}_1^0 \rightarrow \gamma\tilde{G}$. We produce all combinations of $\tilde{\chi}_i^\pm$ and $\tilde{\chi}_j^0$, which are the only significant cross sections. We vary Λ which varies the overall mass scale of the supersymmetric particles.

The model masses and branching ratios are given in Table XIV. The branching ratio is defined as the number of events with $\tilde{\chi}_1^0 \rightarrow \gamma\tilde{G}$ and $\tilde{\chi}_1^0 \rightarrow h\tilde{G}$ divided by the number of events produced from all sources predicted by the model. We are using `ISAJET` with the CTEQ4L parton distribution function. The first point appears to have an unusually large efficiency because of other sources for b quarks which are not reflected in the definition of the signal branching ratio. We use the systematic uncertainties evaluated using the direct production of the $\tilde{\chi}_2^0 \rightarrow \gamma\tilde{\chi}_1^0$ model.

Taking the two events observed, and convoluting with a 20% systematic uncertainty gives an upper limit of 6.4 events observed at 95% C.L. The final limits on this model are presented in Table XV and displayed in Figure 11. Again, one can see that the experimental sensitivity is not adequate to set a mass limit (this time on the $\tilde{\chi}_1^\pm$ mass) by several orders of magnitude.

$M_{\tilde{\chi}_1^0}$,	$M_{\tilde{\chi}_2^0}$	$M_{\tilde{\chi}_1^\pm}$	$BR(\tilde{\chi}_1^0 \to \gamma\tilde{G})$	$BR(\tilde{\chi}_1^0 \to h\tilde{G})$
113	141	130	90	2
132	157	147	62	18
156	178	170	33	40
174	194	186	22	50

TABLE XIV. The models used in the limits on the GMSB scenario. The lightest Higgs boson is 100 GeV. The masses are in GeV and the branching ratios are in %.

$A\epsilon$	BR	$\sigma_{th} \times BR$	$\sigma_{95\%\ lim} \times BR$
27.4	3	0.010	0.27
7.5	20	0.0402	1.00
8.4	23	0.0230	0.89
11.4	18	0.0111	0.66

TABLE XV. Efficiencies and limits on direct production of $\tilde{\chi}_i^\pm \tilde{\chi}_j^0$ in the GMSB scenario. Branching ratios are not included in these efficiencies. The first row has an inflated efficiency due to the definition of the branching ratio. The units of $A\epsilon$ and the branching ratio are % and the cross sections are in pb.

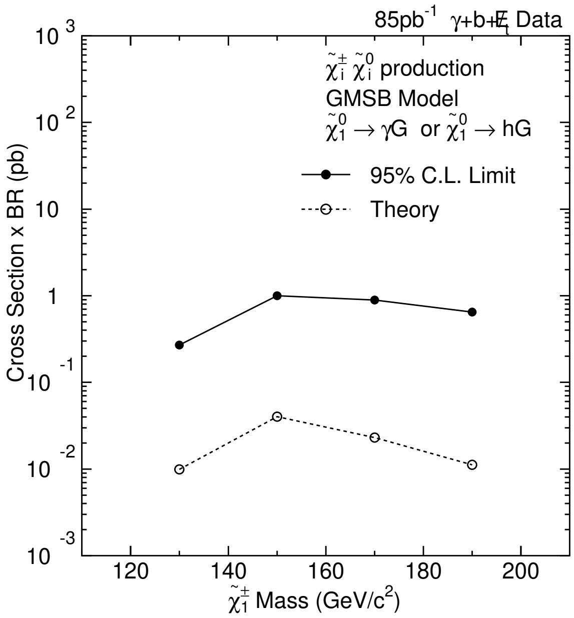

FIG. 11. The limits on the cross section times branching ratio for SUSY production of $\gamma b \not\!\!E_t$ events in the GMSB model. All production processes have been included.

VI. MODEL–INDEPENDENT LIMITS

As described in the introduction, there are several advantages to presenting limits of searches in a model–independent form. In the previous sections we derived limits on models of supersymmetry and presented the results as a limit on a cross section times branching ratio for a specific model, $(\sigma \times BR)^{lim} = N^{lim}/\mathcal{L}A\epsilon$, where N_{lim} is the 95% confidence level on the number of events of anomalous production and $\mathcal{L}$ is the integrated luminosity. We make a distinction between the acceptance, A, which is defined as probability that an object passes E_t, η, and $\Delta\phi$ cuts, and the efficiency, ϵ, which is the probability of events surviving all other sources of inefficiencies, such as photon identification cuts or b–tagging requirements, which is detector-specific. The acceptance may be calculated from kinematic and geometric criteria alone, so an experienced worker in the field can compute it using only a Monte Carlo event generator program, while the efficiency requires access to the full detector simulation and, typically, multiple control samples. In our formulation, N_{lim} includes the degradation in sensitivity due to uncertainties on $A\epsilon$, luminosity, and background subtractions, when they are included, as well as the statistical upper limit on the number of events.

In the case of model–independent limits, there is no model to determine the efficiency and therefore we report a limit on $(\sigma \times BR \times A\epsilon)^{lim} = N^{lim}/\mathcal{L}$. These limits, which are presented in the next section, do not have an immediate interpretation. (They do imply, however, a cross section range that we are *not* sensitive to, even with perfect efficiency.) In order to determine the meaning of these limits, in particular if a model is excluded or not, there must still be a mechanism for an interested physicist to calculate $A\epsilon$ for the model, and we develop three methods in the Appendix.

A. Model–independent Limits on γbX Signatures

The limit on $(\sigma \times BR \times A\epsilon)_i^{lim} = N^{lim}/\mathcal{L}$ is described by reporting that two events are observed with an isolated photon with E_t >25 GeV and $|\eta| < 1$, a SVX-tagged b–quark jet with E_t >30 GeV and $|\eta| < 2$, $\Delta\phi(\gamma - \not\!\!E_t) < 168°$ and $\not\!\!E_t > 40$ GeV. The cuts are fully described in Section II. The integrated luminosity for this sample is (85 ± 3) pb^{-1}.
The resulting 95% confidence level limit on $(\sigma \times BR \times A\epsilon)^{lim}$ for the $\gamma b \not\!\!E_t$ signature is then 0.069 pb. Adding the 4% luminosity uncertainty we find the cross section limit increases to 0.070 pb. If we also add the 22% uncertainty in $A\epsilon$ from the WW limits (a typical uncertainty on an efficiency for this signature) discussed in the Appendix, we find the cross section limit increases 10% to 0.077 pb. This is the final model–independent limit on the signature $\gamma b \not\!\!E_t$.

The limit on the γb signature before any $\not{E}_t$ requirement is 5.9 pb and the limit from the $\gamma b \not{E}_t$ signature from the 98–event sample with $\not{E}_t > 20$ GeV is 0.99 pb.

The search for other objects in these events is described in Sections II E and IV C. When we find no events, we can set a 95% confidence level limit on $(\sigma \times BR \times \epsilon A)^{lim}$ of 0.038 pb assuming 4% uncertainty in the luminosity and 22% uncertainty in the efficiency. This would apply to the searches for events with an additional photon, a muon or tau. For events with an additional electron, we observe one event and our limit becomes 0.057 pb.

For events with N or more jets as shown in Figure 7, we find the limits listed in Table XVI.

N	$\sigma_{lim}^{95\%}$ (pb), $\not{E}_t > 0$ GeV	$\sigma_{lim}^{95\%}$ (pb), $\not{E}_t > 20$ GeV
1	5.9	0.99
2	2.5	0.77
3	1.5	0.50
4	0.52	0.18
5	0.24	0.10
6	0.14	0.062
7	0.083	0.038
8	0.062	0.038

TABLE XVI. The 95% confidence level limits on $(\sigma \times BR \times \epsilon A)^{lim}$ in pb for events with N or more jets, including the b jet.

VII. CONCLUSIONS

We have searched in 85 pb^{-1} of CDF data for anomalous production of events with a high–E_t photon and a b–tagged jet. We find 1175 events with a photon with $E_t > 25$ GeV and a b–tagged jet with $E_t > 30$ GeV, versus 1040±186 expected from standard model backgrounds. Further requiring missing transverse energy $\not{E}_t > 40$ GeV, in a direction not back-to-back with the photon ($\Delta\phi < 168°$), we observed 2 events versus 2.3± 1.6 events expected. In addition we search in subsamples of these events for electrons, muons, and tau-leptons, additional photons, jets and b–quark jets. We conclude that the data are consistent with standard model expectations.

We present limits on three current models of supersymmetry. The first is indirect production of chargino-neutralino pairs through squark and gluino production, where the photon is produced in $\tilde{\chi}_2^0 \to \gamma\tilde{\chi}_1^0$ and the b-quark comes from the chargino decay into the light stop squark $\tilde{\chi}_1^+ \to \tilde{t}b$. A choice of favorable values of the parameters allows setting a lower mass limit on the gluino mass of 250 GeV. The second model is similar, but we look only at direct production of the $\tilde{\chi}_2^0\chi_2^\pm$ pair. A cross section limit of $\sim$ 7-10 pb is set, but is above the predictions for all $\tilde{\chi}_2^0$ masses so that no mass limit can be set. Lastly, a GMSB model is considered in which the photon comes from the decay $\tilde{\chi}_1^0 \to \gamma\tilde{G}$. Limits in the range 0.3-1.0 pb are set versus the mass of the $\tilde{\chi}_1^0$, but again no mass limit can be set as the cross section predictions are lower than the limit.

Finally, we present a model–independent limit of 0.077 pb on the production of events containing the signature $\gamma b \not{E}_t$, and propose new methods for applying model–independent limits to models that predict similar broad signatures. We conclude that an experienced model–builder can evaluate whether model-independent limits apply to a particular model with an uncertainty of approximately 30%.

VIII. ACKNOWLEDGMENTS

We thank the Fermilab staff and the technical staffs of the participating institutions for their vital contributions. This work was supported by the U.S. Department of Energy and National Science Foundation; the Italian Istituto Nazionale di Fisica Nucleare; the Ministry of Education, Science, Sports and Culture of Japan; the Natural Sciences and Engineering Research Council of Canada; the National Science Council of the Republic of China; the Swiss National Science Foundation; the A. P. Sloan Foundation; the Bundesministerium fuer Bildung und Forschung, Germany; the Korea Science and Engineering Foundation (KoSEF); the Korea Research Foundation; and the Comision Interministerial de Ciencia y Tecnologia, Spain.

IX. APPENDIX: APPLICATION OF MODEL–INDEPENDENT LIMITS

In the body of this paper, we present the limits on specific models of new physics that predict the $\gamma b \not\!\!E_t$ signature, then rigorously calculate $A\epsilon$ for that model by using a Monte Carlo with a full detector simulation. We present our limits on $(\sigma \times BR)^{lim} = N^{lim}/\mathcal{L}A\epsilon$, or a parameter of the model such as the mass of a supersymmetric particle.

A new paradigm, the signature–based or, equivalently, model–independent search may be an effective method for reporting the results of searches in the future. In this case, a signature, such as the photon and b–quark jet addressed in this paper, is the focus of the search rather than the predictions of a particular model.

There are several advantages to this approach [1,3,4].

1. The results are not dated by our current theoretical understanding.
2. No *a priori* judgement is necessary to determine what is an interesting model.
3. The results more closely represent the experimental observations and results will be presented in a form that can be applied to a broad range of models including those not yet imagined.
4. The number of signatures is more reasonably limited than the number of models and model parameters.
5. Concentrating on a particular model can tend to focus the search very narrowly, ignoring variations on the signature which may be just as likely to yield a discovery.
6. Time spent on studying models can be diverted to systematically searching additional signatures.

In order to reflect the data results more generally, in the body of this paper we also present a limit on $(\sigma \times BR \times A\epsilon)^{lim} = N^{lim}/\mathcal{L}$ for the signatures with no calculation of $A\epsilon$. With limits presented this way, the collaboration itself, model–builders and other interested workers are no longer given limits on the physics models directly but now must derive the limits themselves. This has the potential for a wider application of the limits. In a pratical sense, it means the interested workers must calculate $A\epsilon$ for the model under study.

In this Appendix, we present three methods to calculate $A\epsilon$. These results together with the model-independent limits can be used to set limits on most models that predict events with the $\gamma b \not\!\!E_t$ signature.

The three methods are referred to as "object efficiencies", "standard model calibration process," and "public Monte Carlo". In the sections below we describe each in turn. In the following sections, we test these methods by comparing the results of each $A\epsilon$ calculation to the rigorously–derived $A\epsilon$ for the specific supersymmetry models.

A. Object Efficiencies

The first method for deriving $A\epsilon$ to use in conjunction with the model–independent limits is object efficiencies. The person investigating a model would run a Monte Carlo generator and place the acceptance cuts on the output which will determine the acceptance, A. The next step would be to apply efficiencies (simple scale factors) for the identification of each object in the signature, such as the photon or the b-quark tag. This has the advantage of being being very straightforward and the disadvantage that correlations between the objects in the event are not accounted for. For example, a model with many jets would tend to have a lower efficiency for the photon isolation requirement than a model with few jets and this effect would not be reflected in this estimate of the efficiency.

Using a sample of $Z \to e^+e^-$ events to measure the efficiencies of the global event cuts, we find the $z < 60$ cm cut is 92% efficient. The probability of finding no energy out-of-time is 98%. In this case the total global efficiency would be the product of these two efficiencies. In the discussion below, the efficiency of the identification of each object is often listed as efficiencies of several separate steps which should be multiplied to find the total efficiency.

We can also use $Z \to e^+e^-$ events to measure the efficiency of the photon identification cuts. One electron from the Z is required to fire the trigger, but the second electron is unbiased with respect to the trigger. In addition the Z peak indicates the number of true physics events, ideal for measuring efficiencies. Which Z electron is required to pass which set of cuts (trigger or offline) must be effectively randomized to avoid correlations between the two sets of cuts. Requiring the cluster to be far from the boundary of the active area in the calorimeters is 73% efficient [31]. The trigger is 91% efficient, the identification cuts are 86% and the isolation requirement is 77% efficient.

For the b–quark efficiency we use a 70% probability that the jets from the event are contained in the SVX. (This would be 64% if the global event vertex was not already required to have $z < 60$ cm.) We add a 90% probability that the jet was taggable (containing two reconstructed tracks in the SVX, passing p_t cuts) and apply the published [32] tagging probability as a function of the jet E_t which can be summarized as

$$\begin{array}{rll} 0 & \text{for} & E_t < 18 \text{ GeV} \\ 0.35 + 0.00277 * E_t & \text{for} & 18 < E_t < 72 \text{ GeV} \\ 0.6 & \text{for} & E_t > 72 \text{ GeV} \end{array}$$

The missing E_t is found as the vector sum of the noninteracting particles in the event. As long as the missing E_t is large, the resolution on the $\not\!\!E_t$ should not greatly effect the efficiency.

In Section IV C, we searched the events in the γb sample for additional leptons; here we present approximate object efficiencies for those cuts. These requirements and their efficiencies are borrowed from top–quark analyses [11,12] as a representative selection for high–E_t leptons. The efficiencies quoted here are measured in those contexts and therefore they are approximations in a search for new physics. In particular, the isolation efficiency is likely to be dependent on the production model. For example, if a model of new physics contained no jets, then the isolation efficiency is likely to be greater than that measured in top–quark events which contain several jets on average.

For the electron search we require $E_t > 25$ GeV and $|\eta| < 1.0$. Given that an electron, as reported in the output of the Monte Carlo generator, passes these acceptance cuts, the probability that the electron strikes the calorimeter well away from any uninstrumented region is 87%, the probability to pass identification cuts is 80%, and to pass isolation cuts is approximately 87% [31].

For muons we require $p_t > 25$ GeV and $|\eta| < 1.0$. Given that the muon, as reported in the output of the Monte Carlo generator, passes these cuts, the fiducial acceptance of the muon detectors is 48%. Once the muon is accepted, the probability to pass identification cuts is 91%, and to pass isolation cuts is approximately 81%.

Tau leptons are identified only in their one– and three–prong hadronic decays which have a branching ratio of 65%. (Tau semileptonic decays can contribute to the electron and muon searches.) We require that the calorimeter cluster has $E_t > 25$ GeV and $|\eta| < 1.2$ and the object is not consistent with an electron or muon. Given that the τ decays to a one– or three–prong hadronic decay mode and passes the E_t and η requirements, the probability that the tau passes identification and isolation cuts is approximately 57%.

In Section IX D we apply these object efficiencies to the supersymmetry models and compare to the results of the rigorously–derived efficiency to test the accuracy of the results.

B. Standard Model Calibration Process

The second method for determining $A\epsilon$ for a model is the Standard Model process or efficiency model. In this method we select a simple physics model that produces the signature. The model is purely for the purpose of transmitting information about $A\epsilon$ so it does not have any connection to a model of new physics. Since it may be considered a calibration model, it does not have to be tuned and will not become dated. The interested model builder runs a Monte Carlo of the new physics and places acceptance cuts on the output, determining A, the same as the first step in the object efficiencies method. This result is then multiplied by the value of ϵ which is taken to be the same as the value of ϵ which we report here for the standard model process.

We have adopted WW production as our efficiency model. One W is required to decay to $e\nu$ and we replace the electron with a photon before the detector simulation. The second W is forced to decay to bu, so the combination yields the signature $\gamma b \not\!\!E_t$. Since some efficiencies may be dependent on the E_t of the objects in the event, we will vary the "W" mass to present this effect. A model–builder would then choose the efficiency that most closely matches the mass scale of the new physics models.

The $A\epsilon$ for this model is found using the same methods as used for the models of supersymmetry. From the difference in the observed efficiencies in Monte Carlo and data $Z \to ee$ samples, we use a 14% uncertainty on the efficiency of the photon ID and isolation. We use 9% for the b–tagging efficiency uncertainty. The parton distribution function we use is CTEQ4L. Comparing this efficiency to those obtained with the MRSD0$'$ and GRV–94LO parton distribution functions, we find a standard deviation of 5%. Turning off initial– and final–state radiation increases the efficiency by 2% and 23% respectively and we take half these numbers as the systematic uncertainty. Varying the jet energy scale by 10% causes the efficiency to change by 6%. We use an 4% uncertainty for the luminosity. In quadrature, the total systematic is 22%. Table XVII summarizes the results.

M_W	75 GeV	100 GeV	125 GeV	150 GeV	175 GeV
$\epsilon A(\%)$	0.85	2.56	4.86	6.98	8.12
ϵ (%)	11.8	10.7	13.9	15.4	16.5

TABLE XVII. Summary of the efficiencies found for the values of W mass used in the WW calibration model versus the value of the "W" mass.

In Section IX D we apply this method of calculating $A\epsilon$ to the supersymmetry models and compare to the results of the rigorously–derived efficiency to test the accuracy of the results.

C. A Public Monte Carlo

A Monte Carlo event generator followed by a detector simulation is the usual method for determining the efficiency of a model of new physics. However, there is usually considerable detailed knowledge required to run the simulation programs correctly so it is not practical to allow any interested person access to it. But if the simulation is greatly simplified while still approximating the full program, it could become usable for any worker in the field. The model–builder then only has to run this simple Monte Carlo to determine $A\epsilon$.

An example of this kind of detector simulation, called SHW, was developed for the Fermilab Run II SUSY/Higgs Workshop [33]. Generated particles are traced to a calorimeter and energy deposited according to a simple fractional acceptance and Gaussian resolution. A list of tracks is also created according to a simple efficiency and resolution model, and similarly for muon identification. The calorimeter energy is clustered to find jets. Electromagnetic clusters, together with requirements on isolation and tracking, form electron and photon objects. The tagging of b–quarks is done with a simple, parameterized efficiency. At points where object identification efficiencies would occur, such as a χ^2 cut on an electron shower profile, the appropriate number of candidates are rejected to create the inefficiency. The result is a simple list of objects that are reconstructed for each event. This method of determining efficiencies addresses the largest concern not addressed in the previous methods – the correlation of the characteristics of jets in the model with isolation requirements. We note that a highly parameterized Monte Carlo has obvious limitations.

We have used the SHW program to compute efficiencies for the three models considered above. Since the program is tuned to provide the approximate efficiency of the Run II detector, we made a few minor changes to reflect the Run I detector. In particular, we changed the photon fiducial efficiency from 85% to 73% and the offline efficiency from 85% to 60%. We reduced the SVX acceptance along the z axis from 60 cm to 31 cm. Finally, we removed soft lepton b-tagging and added a 90% efficiency for the global event cuts.

In the next section we use the public Monte Carlo to calculate $A\epsilon$ for the supersymmetry models and compare the results to the rigorously–derived efficiency to test the accuracy of the public Monte Carlo.

D. Tests of the Model–independent Efficiency Methods

In the body of this paper we have provided rigorous limits on several variations of three supersymmetry physics models that produce the signature of $\gamma b \not\!\!E_t$. In this section we apply the model-independent efficiency methods to the supersymmetry models. We can then compare the results with the rigorous limits to evaluate how effective it is to apply the model–independent limits to real physics models.

In most cases we need to distinguish between acceptance and efficiency. Acceptance, indicated by A, we define as the probability for generated Monte Carlo objects to pass all geometric and E_t cuts. For the $\gamma b \not\!\!E_t$ signature, with $\not\!\!E_t$ defined as the vector sum of neutrinos and LSP's, the cuts defining the acceptance of the signature are listed in Table XVIII.

γ	$E_t > 25$ GeV	$\lvert\eta\rvert < 1.0$
b–quark	$E_t > 30$ GeV	$\lvert\eta\rvert < 2.0$
Additional Signatures		
$\Sigma p_t(\nu,\ LSP)$	$\not\!\!E_t > 40$ GeV, $\Delta\phi(\gamma - \not\!\!E_t) < 168^\circ$	
e	$E_t > 25$ GeV	$\lvert\eta\rvert < 1.0$
μ	$E_t > 25$ GeV	$\lvert\eta\rvert < 1.0$
τ	$E_t > 25$ GeV	$\lvert\eta\rvert < 1.2$
$2^{\text{nd}}\ \gamma$	$E_t > 25$ GeV	$\lvert\eta\rvert < 1.0$
$2^{\text{nd}}\ b$	$E_t > 30$ GeV	$\lvert\eta\rvert < 2.0$
Jets	$E_t > 15$ GeV	$\lvert\eta\rvert < 2.0$

TABLE XVIII. The list of requirements on the output of a Monte Carlo generator which define the acceptance of a signature, A. The requirements on the photon and b–quark jet above the double line are common to all signatures in this paper. When missing E_t is required, as in all the supersymmetry searches and the tests of model–independent methods, both $\not\!\!E_t > 40$ GeV and $\Delta\phi(\gamma - \not\!\!E_t) < 168^\circ$ are required. The $\not\!\!E_t$ requirement is removed and other requirements are added to make specific subsamples.

Table XIX and Figure 12 list the results. The columns marked R are the efficiency times acceptance done rigorously, divided by the the same found using each of the model–independent methods. The difference of this ratio from 1.0 one is a measure of the accuracy of the approximate methods compared to the rigorous method.

Model	M_s	BR(%)	A	$A \cdot \epsilon$	R_{obj}	R_{WW}	R_{SHW}
GMSB $M_s = M_{\tilde{\chi}_1^\pm}$	130	3	65.0	27.50	2.79	3.03	1.07
	147	20	49.8	7.45	0.91	1.00	0.70
	170	23	51.7	8.35	0.97	1.00	0.87
	186	18	54.7	11.44	1.26	1.22	1.11
$\tilde{\chi}_2^0 \to \gamma\tilde{\chi}_1^0$ $\tilde{q}$, $\tilde{g}$ production $M_s = M_{\tilde{g}}$	185	30	17.0	1.97	0.91	0.68	0.48
	210	30	22.0	2.98	1.04	0.73	0.90
	235	30	24.0	3.23	1.01	0.68	0.90
	260	30	24.5	2.69	0.82	0.52	0.75
	285	30	19.7	2.16	0.84	0.48	0.72
$\tilde{\chi}_2^0 \to \gamma\tilde{\chi}_1^0$ $\tilde{q}$, $\tilde{g}$ production $M_s = M_{\tilde{\chi}_2^\pm}$	110	100	13.5	0.93	0.54	0.54	0.59
	130	100	12.6	1.41	0.88	0.80	0.87
	140	100	14.8	1.29	0.68	0.60	0.66
	150	100	13.7	1.34	0.77	0.65	0.78
	170	100	11.5	1.27	0.85	0.68	0.65

TABLE XIX. The results of comparing the methods of calculating $A\epsilon$ using the model–independent methods and the rigorously–derived $A\epsilon$. Each row is a variation of a model of supersymmetry as indicated by the label in the first column and the mass of a supersymmetric particle listed in column two (GeV). The column labeled A is the acceptance of the model in % and the next column is the rigorously–derived $A\epsilon$. The columns labeled with R are the ratios of the rigorously–derived $A\epsilon$ to $A\epsilon$ found using the model–independent method indicated.

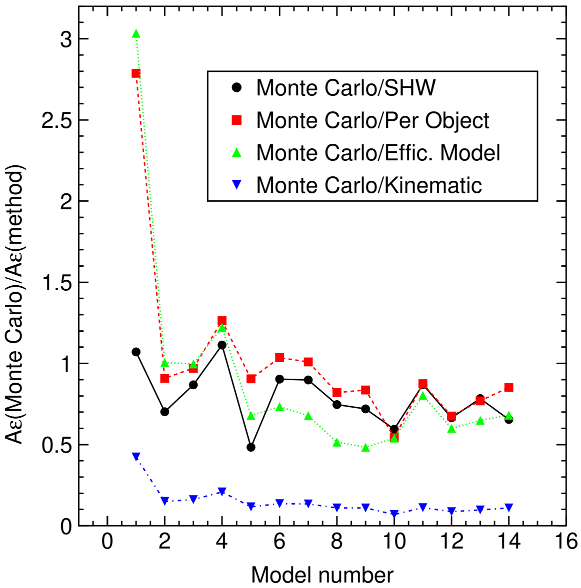

FIG. 12. The ratio of the efficiencies obtained with full detector simulation to those obtained with the model–independent methods. The x axis is the row number from Table XIX.

E. Conclusions from tests

There are several notable effects apparent immediately from Table XIX and Figure 12. The first is that the comparison of efficiencies for one model point fares especially poorly. This occurs when the branching ratio for the model is very small (2%). When the events do not contain many real photons and b quarks, the small number of objects misidentified as photons and b-quarks becomes important. For example, jets may pass photon cuts and c quarks may be b-tagged. When this occurs, the full simulation will be more efficient than a method which specifically requires that the Monte Carlo generate an isolated photon or b-quark in order to accept the event. This is true of the object efficiencies method and the efficiency model method. We note that the public Monte Carlo method does allow misidentification and so it does not show this large mismatch. We can conclude that when the branching ratios are small, the public Monte Carlo method is vastly superior to the others.

In the object efficiency method, the acceptance of the signature is computed by running the Monte Carlo without a detector simulation. As each object in the signature is identified and passes acceptance cuts, the individual object efficiencies are multiplied. These object efficiencies which may or may not be E_t– or η–dependent, are listed in Section IX A. In this test, these efficiencies are typically well–matched to the rigorously–derived efficiencies. The average of R_{obj} over all models except the first, is 0.88 ± 0.21 where 0.21 is the RMS computed with respect to 1.0, the ideal result.

In the efficiency model method, we generate a Monte Carlo model that is not related to a search for new physics but produces the signature of interest. For the signature of $\gamma b \not\!\!E_t$, we generated $WW \rightarrow (\gamma\nu)(bu)$. The efficiency model results are also optimistic, the average is a ratio of 0.74 ± 0.35 where again the uncertainty is actually the RMS with 1.0, the ideal result. We found that the difficulty of applying this method was in choosing the mass scale. For example, we chose to match the "W" mass to the $\tilde{\chi}_2^{\pm}$ mass in the direct production of the $\tilde{\chi}_2^0 \rightarrow \gamma\tilde{\chi}_1^0$ model. However, the photon comes from a secondary decay and the effect of the LSP mass compared to the massless neutrino causes the E_t of the γ and b to be poorly matched to the E_t of these objects in the WW model.

In the public Monte Carlo method, we compute the efficiency using SHW, a highly-parameterized, self–contained Monte Carlo. In general, results here are somewhat optimistic with the average ratio to the rigorous total efficiency being 0.77 ± 0.28, where the uncertainty is the RMS computed with respect to 1.0, the ideal result.

For completeness we also include the ratio of the simple acceptance to the rigorous acceptance times efficiency. The average ratio is 0.12 ± 0.87.

The methods for calculating efficiency without access to the full detector simulation are accurate to approximately 30% overall. They tend to underestimate $A\epsilon$ by 10-25% but the result for individual comparisons varies greatly. These uncertainties are larger than, but not greatly larger than, a typical uncertainty in a rigorously–derived efficiency, which is 20%.

We conclude that to determine if a model is easily excluded or far from being excluded by the data, the model–independent methods are sufficient. If the model is within 30% of exclusion, no conclusion can be drawn and the efficiency should be rigorously–derived.

[1] F. Abe *et al.* (The CDF Collaboration), Phys. Rev. Lett. **81** 1791 (1998), Phys. Rev. D **59** 092002,1999.
[2] S. Ambrosanio, G.L. Kane, Graham D. Kribs, Stephen P. Martin, and S. Mrenna, Phys. Rev. Lett. **76**, 3498 (1996); G. L. Kane and S. Mrenna, Phys. Rev. Lett. **77**, 3502 (1996); S. Ambrosanio, G.L. Kane, Graham D. Kribs, Stephen P. Martin, and S. Mrenna, Phys. Rev. D **55**, 1372 (1997).
[3] H. Frisch, in proceedings of the NATO Summer School 1998, Cargese, France, to be published, edited by P. Binetruy ad G. Smadja (Kluwer Academic Publishers).
[4] B. Abbott *et al.* (The DO Collaboration), Phys. Rev. D **62**, 92004 (2000); B. Abbott *et al.* (The DO Collaboration), Phys. Rev. Lett., **86**, 3712 (2001); B. Abbott *et al.* (The DO Collaboration), to be published in Phys. Rev. D, hep-ex/0011067 (2000).
[5] F. Abe *et al.* (The CDF Collaboration), Phys. Rev. Lett **83**, 3124 (1999).
[6] F. Abe *et al.* (The CDF Collaboration), Nucl. Instrum. Methods Phys Res., Sect. A **271**, 387 (1988).
[7] D. Amidei *et al.*, Nucl. Instrum. Methods Phys. Res., Sect. A **350**, 73 (1994).
[8] The CDF coordinate system is right-handed, and has the z axis aligned with the proton beam and y vertical. The azimuthal angle is denoted as ϕ and the polar angle as θ; η is $-\ln[\tan(\theta/2)]$.
[9] D. Amidei *et al.*, Nucl. Instrum. Methods Phys. Res., Sect. A **269**, 51 (1988).
[10] F. Abe *et al.* (The CDF Collaboration), Phys. Rev. D **45**, 1448 (1992).
[11] F. Abe *et al.* (The CDF Collaboration), Phys. Rev. Lett. **74** 2626 (1995); Phys. Rev. D **50**, 2966 (1994).
[12] F. Abe *et al.* (The CDF Collaboration), Phys. Rev. Lett. **79**, 3585 (1997).
[13] F. Abe *et al.* (The CDF Collaboration), Phys. Rev. Lett. **73**, 2662 (1994); Phys. Rev. D **48**, 2998 (1993).
[14] F. Abe *et al.* (The CDF Collaboration), Phys. Rev. D **50**, 2966 (1994); Phys. Rev. Lett. **73**, 225 (1994).
[15] The $\gamma b\bar{b}$ and $\gamma c\bar{c}$ Monte Carlo program was incorporated into Herwig by M. Mangano, based on calcuations in R. K. Ellis and Z. Kunszt, Nucl. Phys. B **303**, 653 (1988); R. K. Ellis and P. Nason, Nucl. Phys. B **312**, 551 (1989).
[16] F. Abe *et al.* (The CDF Collaboration), Phys. Rev. Lett. **73**, 2662 (1994).
[17] In this Letter when two uncertainties are reported, the first is statistical and the second is systematic.
[18] J. Breitweg *et al.* (The ZEUS Collaboration), Z. Phys. **C74** 207, 1997. A similar method was developed in C. Adloff *et al.* (The H1 Collaboration), Z. Phys. **C74** 191, 1997.
[19] For an introduction to SUSY, see, for example: M. Carena, R.L. Culbertson, S. Eno, H.J. Frisch, and S. Mrenna, *The Search for Supersymmetry at the Tevatron Collider*, Rev. Mod. Phys. 71, no.4 (July 1999).
[20] T. Sjostrand, Computer Physics Commun. **82**, 74 (1994). We use Version 6.1.
[21] S. Abachi *et al.* (The DO Collaboration), Phys. Rev. Lett. **76** 2222 (1996); G. Abbiendi *et al.* (The OPAL Collaboration), Phys. Lett. B **456**, 95 (1999); P. Abreu *et al.* (The Delphi Collaboration), Phys. Lett. B **496**, 59 (2000); M. Acciarri *et al.* (The L3 Collaboration), Phys. Lett. B **471**, 308 (1999); R. Barate *et al.* (The Aleph Collaboration), Phys. Lett. B **434**, 189 (1998).
[22] T. Affolder *et al.* (The CDF Collaboration) Phys. Rev. Lett. **84**, 5704 (2000).
[23] H. L. Lai *et al.* (The CTEQ collaboration), Phys. Rev. D **55**, 1280 (1997).
[24] A. D. Martin, R. G. Roberts, and W. J. Stirling, Phys. Lett. B **306**, 145 (1993).
[25] M. Gluck, E. Reya, and A. Vogt, Z. Phys. C **67**, 433 (1995).
[26] O. Helene, Nucl Instrum. Methods Phys. Res., Sect. A **212**, 319 (1983).
[27] G. Zech, Nucl Instrum. Meth. A **277**, 608 (1989).
[28] W. Beenaker, R. Hopker, and M. Spira, hep–ph/9611232 (1996).
[29] For an introduction to gauge-mediated SUSY, see, for example: S. Dimopoulos, S. Thomas, and J. D. Wells, Nucl. Phys. B **488** 39 (1997); R. L. Culbertson *et al.*, hep–ph/0008070 (2000).
[30] H. Baer *et al.*, Proc. of the Workshop on Physics at Current Accelerators and the Supercollider, Argonne, 703 (1993). We are using Version 7.37.
[31] D. Toback Ph.D. thesis, University of Chicago, 1997.
[32] Weiming Yao, in *New Directions for High–Energy Physics,* proceedings of 1996 DPF / DPB Summer Study on New Directions for High–energy Physics (Snowmass 96), Snowmass, CO, edited by D.G. Cassel and L. Trindle (Stanford, CA, Stanford Linear Accelerator Center, 1997. 2v.).
[33] The Supersymmetry/Higgs Workshop, Fermilab, Batavia IL, November 19, 1998. http://fnth37.fnal.gov/susy.html.